EARTHQUAKE HISTORY, MICROSTRUCTURE, AND FAULT FRICTIONAL PROPERTIES OF NEAR-SURFACE SEDIMENTS ON THE NORTHERN SAN ANDREAS FAULT AT ALDER CREEK, CALIFORNIA

By

Ryan Crawford

A Thesis

Presented to the Faculty of Humboldt State University

in Partial Fulfillment

of the Requirements for the

Degree Master of Science

Environmental Systems

Geology

May 2007

EARTHQUAKE HISTORY, MICROSTRUCTURE, AND FAULT FRICTIONAL PROPERTIES OF NEAR-SURFACE SEDIMENTS ON THE NORTHERN SAN ANDREAS FAULT AT ALDER CREEK, CALIFORNIA

By

Ryan Crawford

Approved by the Master's Thesis Committee:

Sue Cashman, Major Professor Date

Mark Hemphil-Haley, Committee Member Date

Mark Rizzardi, Committee Member Date

Sharon Brown, Graduate Coordinator Date

Chris Hopper, Dean for Research and Graduate Studies Date

ABSTRACT

Ryan Crawford

Brittle deformation of young unconsolidated sediments related to recent faulting events is not well understood. Deformation bands in Late Holocene fluvial sands overlying the active trace of the San Andreas Fault (SAF) were studied to examine the relationship between faulting and deformation band development.

Methods used include: trenching and logging the known 1906 SAF rupture trace, taking detailed oriented deformation band and control samples, experimental deformation of sand samples away from the active SAF trace to determine fault mechanical properties, and comparison of microstructures in deformation bands found in the SAF to experimental microstructures within the experimentally deformed samples.

Deformation bands and experimentally deformed sand exhibit very similar preferential grain orientations that are not observed in control samples. Deformation band and control sand grain orientations are statistically unique populations. Deformation bands have lower porosity and smaller grain-size compared with control sands. The sand has a high coefficient of friction that increases with accelerated strain-rate at near-surface conditions. Experimental work shows velocity-strengthening characteristics.

I conclude from frictional and fault mechanical properties of sand at the study site that new deformation band development most likely do not reoccupy older deformation

band shear planes. Deformation band formation is a lithologically and compositionally controlled process that changes the grain-size, grain orientation, and strength of the original sediment.

ACKNOWLEDGEMENTS

My greatest thanks go to Dr. Sue Cashman (Humboldt State University, Department of Geology Faculty) as principle investigator to NSF grant EAR0408790 for taking me in as a Masters student within the project. Not only for her input on the thesis scientifically and theoretically, but also for valuable direction, support, embracing new ideas, and for giving me geological fundamentals at my undergraduate and graduate levels of study.

I would like to express my gratitude to John Baldwin (William Lettis & Associates) for his encouragement to work on this study, his inspirational modesty in his present and previous paleoseismology work, as well as his field expertise in the trenches.

I am very thankful to the entire Humboldt State University Geology Department faculty and staff for their support, encouragement, and belief in my abilities over the years. Especially; Scott North for his knowledge of artificially consolidating materials in thin-section preparation; John Longshore for petrological and compositional insight; Mark Hemphil-Haley for his role as a thesis committee member and incredible gift to grasp the big picture; and Andre Lehre for crucial thesis advise and teaching me rigorous quantification skills. I also thank Professor Mark Rizzarti (Humboldt State University, Mathematics Department) for his role in statistical guidance and enthusiasm as a thesis committee member.

I am also very thankful to Dr. Kathy Cashman (University of Oregon, Department of Geological Sciences) for her help and access to the department's Scanning Electron

Microscope (SEM) and for her hospitality. Also, I would like to thank John Donovan (University of Oregon, Department of Geological Sciences) for his technical expertise with the SEM and related equipment.

I am particularly grateful to Dr. Chris Marone (Penn State, Geosciences Faculty) for not only rousing my interest and potential for fault mechanical properties in this study, but for welcoming me into their world class Rocks Mechanics Laboratory, and opening his wealth of knowledge of frictional data interpretation to me. Additionally, from Penn State I would like to thank Brett Carpenter for his critical help in constructing and experimentally deforming Alder Creek sand.

Finally, I would like to express my appreciation to the Stornetta family of Manchester, California for permission to conduct this investigation on their lovely portion of the San Andreas Fault.

TABLE OF CONTENTS

LIST OF TABLES

LIST OF FIGURES

INTRODUCTION

I studied deformation on the North Coast segment of the San Andreas fault (SAF) at Alder Creek, California (Figure 1) along the 1906 earthquake rupture. This site was selected for a study of microstructures produced by coseismic slip because of its well-documented earthquake history and because of the presence of suitable well-sorted sands.

The first objective of this study was to examine the earthquake chronology to see if it could be further refined. The second objective was to find and describe microstructures of the 1906 earthquake at the outcrop-scale at Alder Creek. The third objective was to determine frictional and fault mechanical properties of sand from the Alder Creek site using laboratory simple-shear tests. The final objective of the study was to compare microstructures from the SAF at Alder Creek to those generated from laboratory tests on the same material.

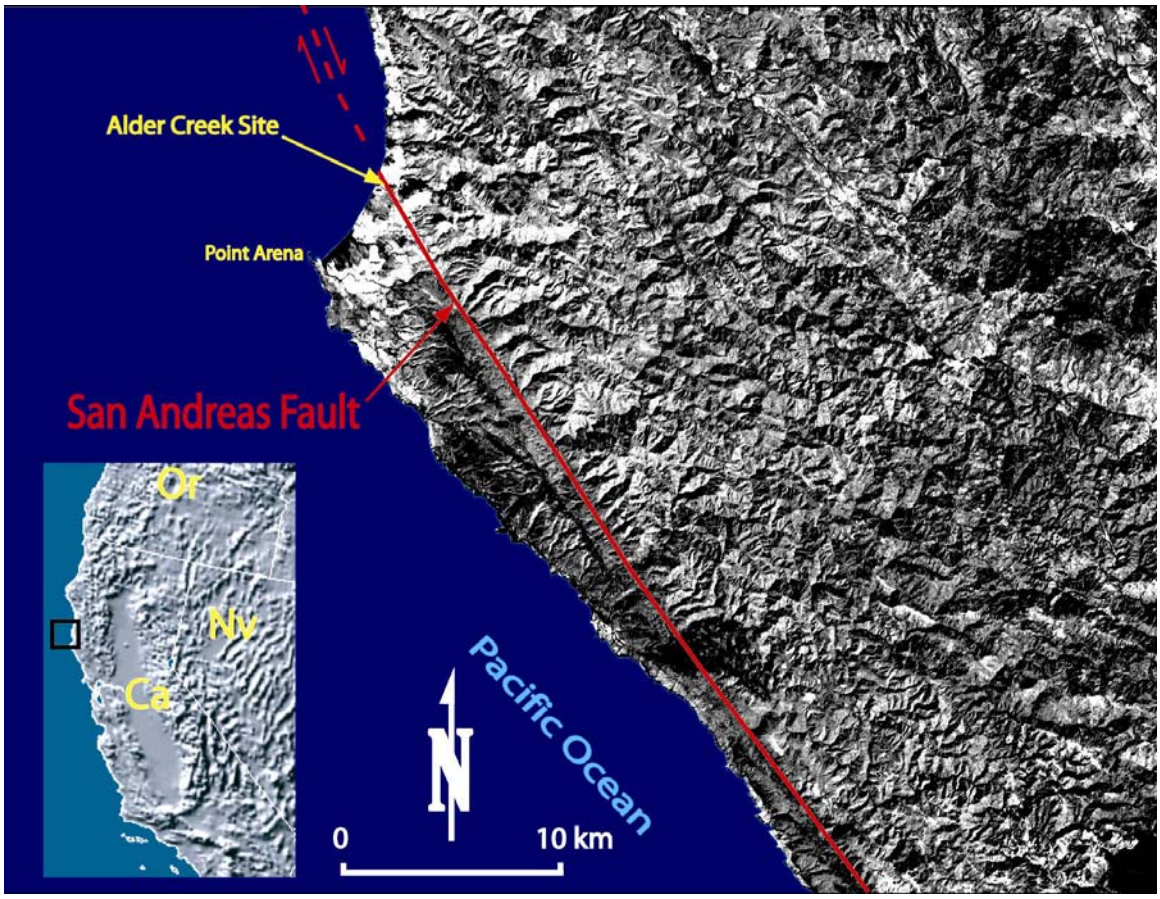

Figure 1. Satellite image of the northern end of the North Coast Segment of the San Andreas Fault along the approximate 1906 earthquake rupture (in red) with the Alder Creek site. Red arrows indicate relative plate motion.

PREVIOUS WORK: REGIONAL GEOLOGY AND TECTONIC SETTING

The SAF is a major transform fault system on the boundary between the Pacific and North America plates. From south to north for a distance of 1300 km, the SAF spans from the Salton Sea in southern California up to Cape Mendocino, California, as right-lateral strike-slip motion typically within a 50-200 km wide swath (Figure 2). Overall plate rate motion between the Pacific-North America Plates is about 49 mm/yr (DeMets et al, 1987) however, integrated relative displacement rates across the SAF zone indicates that it accommodates about 70-80% of the motion at a maximum of 33-37 mm/yr (Thatcher, 2006). Although the SAF has both seismic (locked) and aseismic slip (constant displacement), the majority of geodetically measured deformation represents strain accumulation within the crustal blocks on either side of the SAF (Thatcher, 2006).

The northern SAF is divided into four principle segments (WGCEP, 2003), the North Coast segment of the SAF consists of the Santa Cruz Mountains segment from San Juan Bautista to Los Gatos, the Peninsula segment from Los Gatos to the Golden Gate, the North Coast segment from the Golden Gate to Alder Creek near Point Arena, and the Offshore segment from Alder Creek near Point Arena Cape Mendocino (Figure 3). Segments have been characterized according to kinematic (geometry and structure) and dynamic (timing, rupture length, and previous earthquake displacements) observations. Although the M_w 7.7 1906 earthquake spanned the four segments of the northern SAF with over 300 km of surface rupture, model derived slip distribution along individual

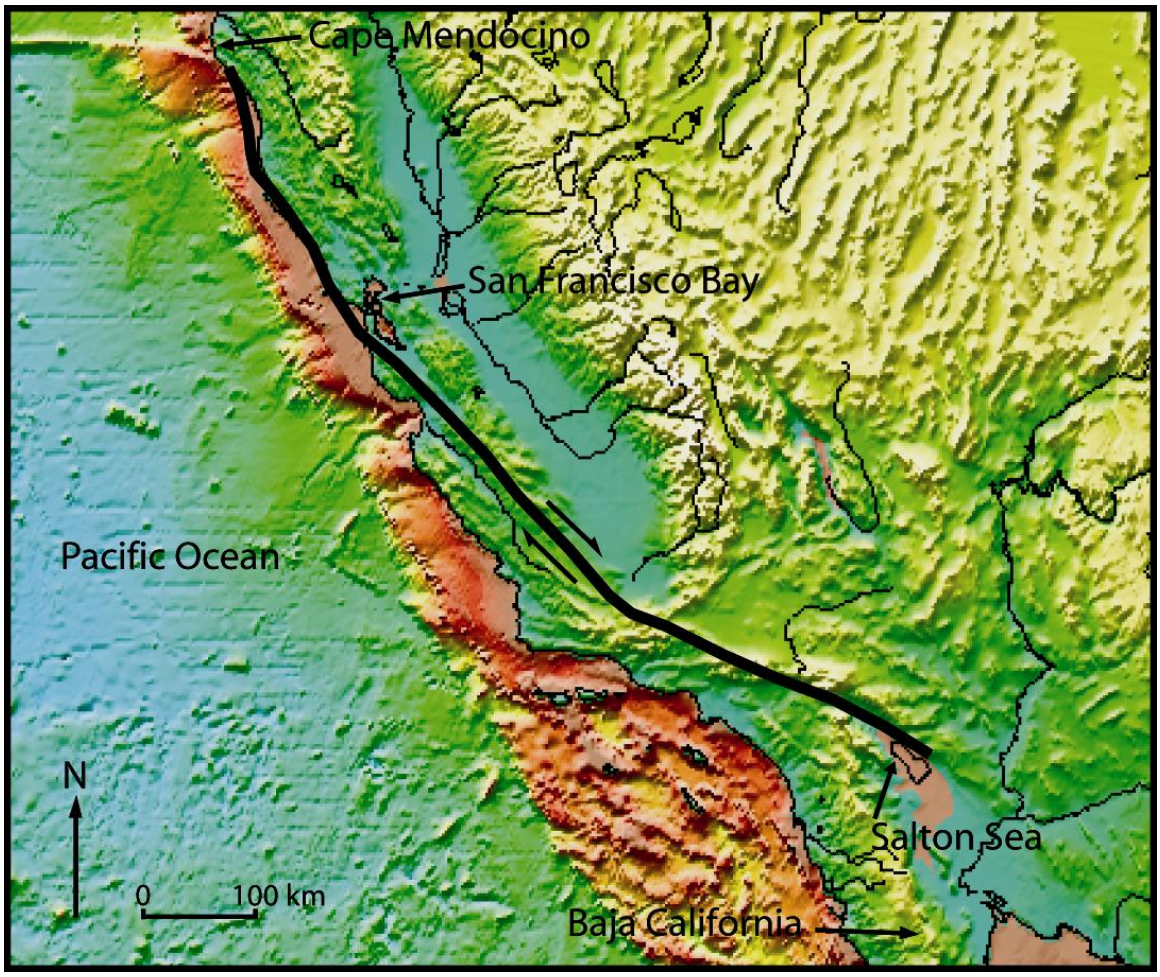

Figure 2. Digital elevation model image showing the extent of the San Andreas Fault. Arrows indicate relative motion.

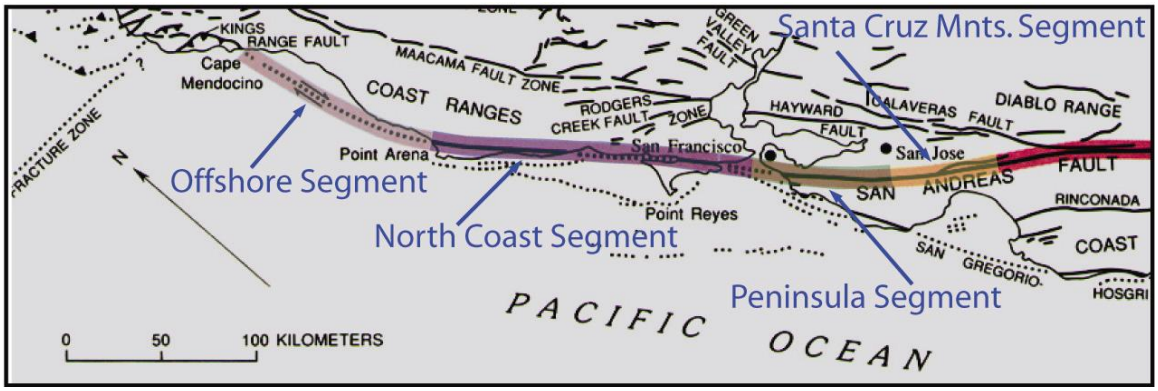

Figure 3. The North Coast segment of the San Andreas Fault divided into the four principle segments with related faults (redrawn after Wallace, 1990).

segments range from zero on the Offshore and Peninsula segments to ±1.0 m on the remaining segments (Thatcher et al, 1997).

The North Coast segment had some of the largest surface ruptures recorded and modeled from the 1906 event. About 1.2 km south of Alder Creek (Figure 4) 4.9 m of right-lateral motion was documented soon after the 1906 event (Lawson, 1906), and 5.9 m of modeled coseismic slip (Thatcher et al, 1997). After almost twenty years of no measurable creep recorded near Alder Creek, coseismic slip remains the only form of seismogenic motion observed at the site (Galehouse, 2002).

The Alder Creek study site is underlain by the Coastal Belt of the Franciscan Complex rocks (Davenport, 1984, CDMG, 1:24,000 Map). These rocks include arkosic sandstones, andesitic and quartzofeldspathic greywacke, and lesser amounts of shale, conglomerate, and serpentinite (Blake and Jones, 1981). Coastal Belt sandstone and

greywacke rocks at or near the Alder Creek site range from late Eocene to Late Cretaceous in age (Blake et al, 2002).

Previous mapping and paleoseismic studies have identified several Quaternary units that unconformably overlie Franciscan bedrock units (Baldwin, 1996, Davenport, 1984, Prentice, 1989). Marine terrace deposits on the west side of the SAF are abruptly juxtaposed with fluvial terrace deposits on the east (Prentice, 1989). Fluvial channel deposits meander over the main fault trace and drape exposed Franciscan bedrock (Baldwin, 1996).

The Northern Segment of the SAF consists of two, 1-2 m wide, active traces near Alder Creek (Figure 5) based on mapping, field reconnaissance, and aerial photograph interpretation (Brown and Wolfe, 1972, Prentice, 1989, Baldwin, 1996). Trending N32ºW, both traces obliquely intersect a steep Alder Creek terrace riser. The eastern trace shows a discernable right lateral separation, while the western trace is more subtle with weakly developed geomorphic expression. Baldwin (1996) interpreted the eastern trace as the main fault, and the western trace to be a secondary, older fault trace. Fault normal trenching revealed that marine terrace deposits, on the west side of the fault, are juxtaposed against fluvial sediments in the primary eastern strand; the western strand ruptures through marine sediments only.

Three earthquake events are identified from previous paleoseismic investigations at Alder Creek (Baldwin, 1996, Baldwin et al, 2005); the 1906 event, a mid-1600's penultimate event, and a poorly constrained event ranging from 660-1630 AD.

Additionally, two events have been observed 1.7 km south at Scaramella Ranch (Figure 4) within the time frame 660-1630 AD (Prentice, 1989).

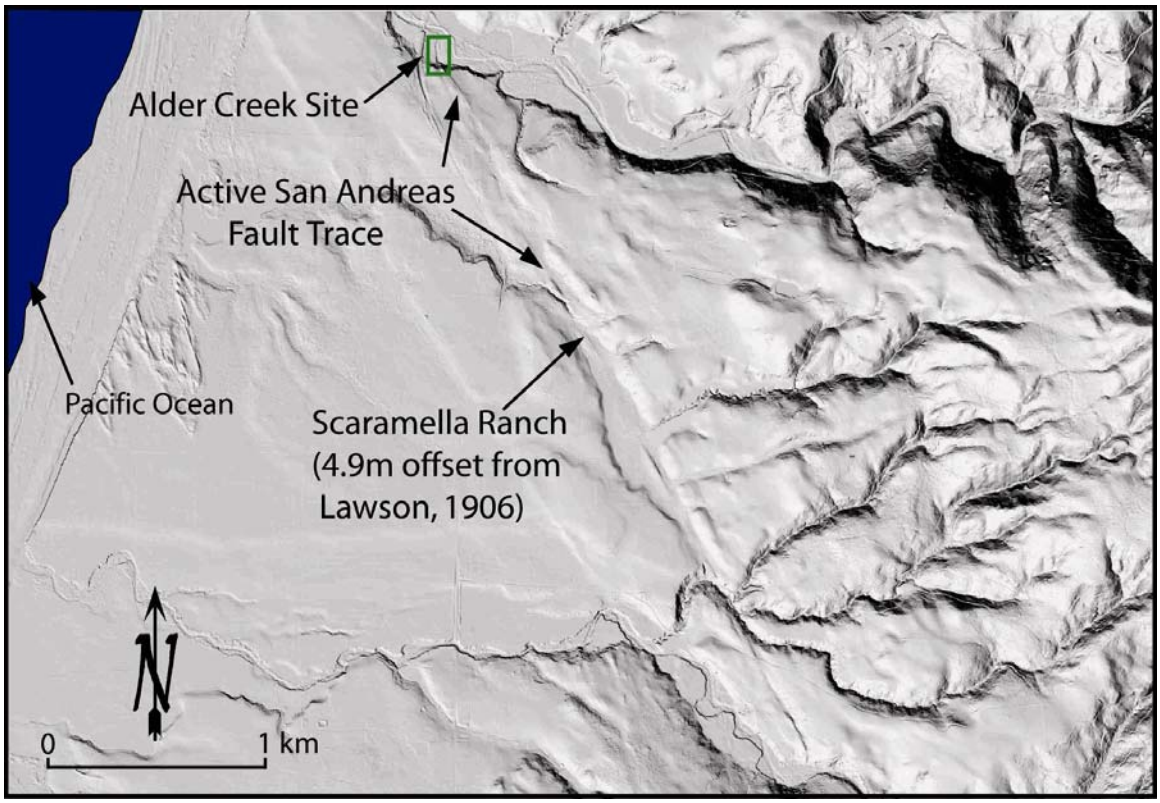

Figure 4. LIDAR image of the Alder Creek site (this study), Scaramella Ranch site, and the site of Lawson's (1906) rupture observation. Note the strong geomorphic expression of the active San Andreas fault through the center of the image.

INVESTIGATIVE APPROACH AND METHODS

Trenching

We excavated two trenches (T-9 and T-10 peal 1, where T-10 was used in a previous study) across the SAF at Alder Creek in July, 2004 (Figure 5). Both trenches were excavated normal to the identified "main eastern trace" of the SAF (Baldwin, 1996, Baldwin et al, 2005). We used data from Baldwin (1996) to target the T-9 site, as there is no present surface expression of the SAF fault immediately above T-9. Trench T-9 was oriented S43°W, and was 2.75 m deep, and 6.75 m long (Figure 6). Trench T-10, also oriented S43ºW, and 2.75 m deep, and almost 9 m long. It was excavated about 4 m northwest of T-9. T-10 Peel 1 was a 4.5 m long, 1.0 m wide cut into the south side and west end of T-10.

We constructed a 1 x 1 m grid on the south trench wall that functioned as a reference for mapping and sample collection. Trench walls were logged at a scale of 1 in.= 0.5 m. Site geologic units were identified based on lithology, stratigraphic position, and inferred age (oldest to youngest). Names and descriptions of sand and gravel units (paleochannels 1-4) are consistent with terminology developed by Baldwin (1996). Only the south wall of T-9 was logged, the north wall contained trench spoils from previous investigations.

The most prominent and representative faults were selected for sampling in trench T-9. Control samples were selected by the following criteria: they came from the same

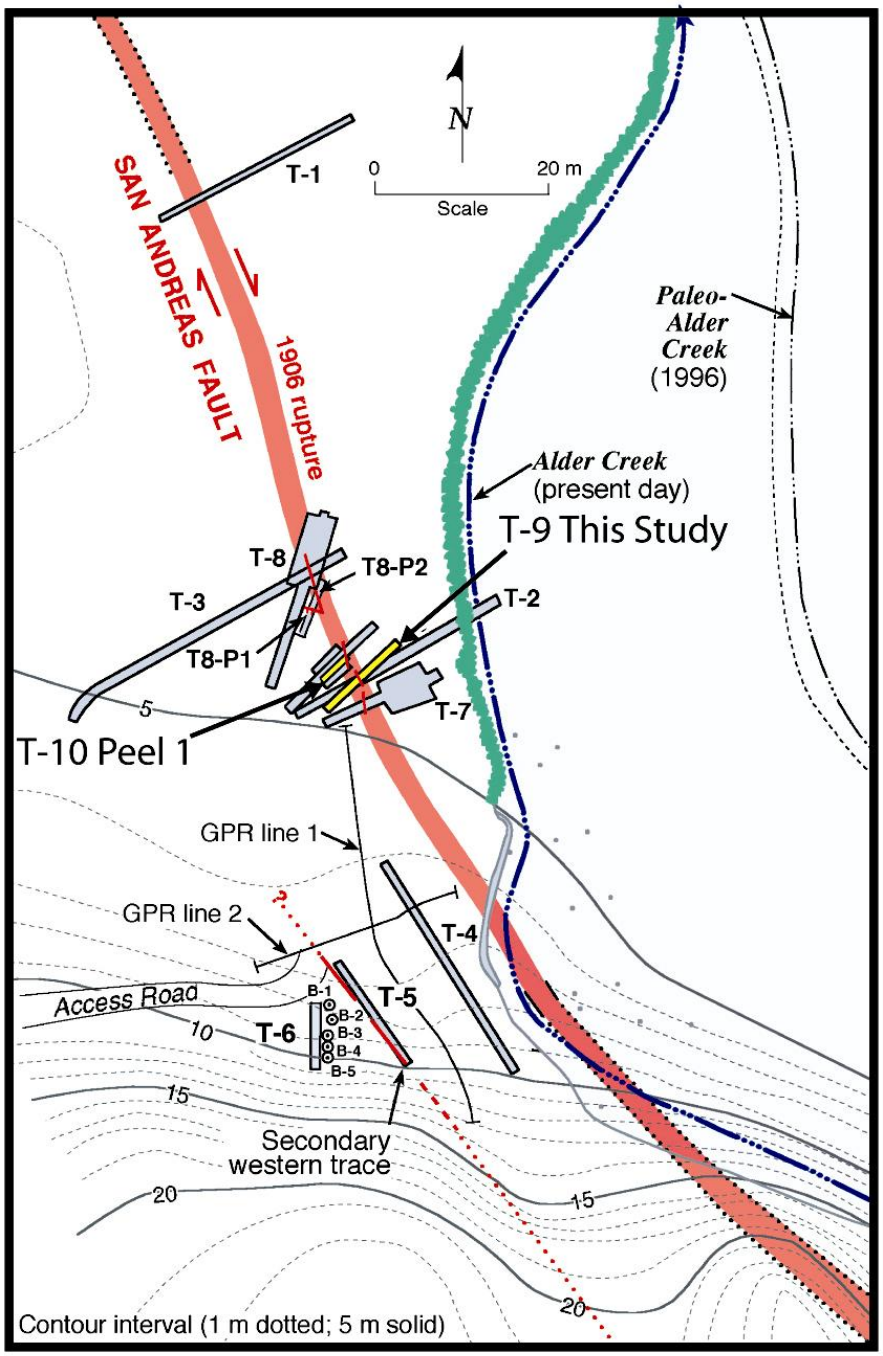

Figure 5. Site topographic map (modified from Baldwin, 2002) showing paleoseismic investigations of this and previous studies indicating trench, ground penetrating radar, boring, and fault locations.

Figure 6. Trench T-9 looking northeast into the hills of the Alder Creek watershed. The willow trees across the upper middle of photo mark the western edge of Alder Creek.

unit as faulted samples, they were selected from the most distal location relative to the faults, and they were from an undisturbed representative sample of the unit. Charcoal samples to be used for potential radiometric ^{14}C data were labeled and wrapped in aluminum foil, then placed in a sealed container.

Analysis of Microstructures

Azimuthally oriented samples for microstructural analysis were collected by pressing 5 x 5 x 2 cm plastic box pairs vertically and horizontally (map view) into the trench wall (following the procedure of Cashman and Cashman, 2000, and Baldwin et al., 2002). Once the box was completely pressed in, it was cut out of the unit with a knife or hand trowel, closed, and sealed tightly with a lid and labeled for orientation and location in the trench. Sample pairs were then brought back to the laboratory and cemented using an epoxy mixture of 100 parts resin to 39 parts hardener by weight. Polished thin-sections were prepared from cemented samples.

Thin-sections were studied using a petrographic microscope and with a FEI Quanta 200 FEG scanning electron microscope (SEM) at the CAMCOR facility, University of Oregon. Six polished thin-sections were scanned with a slide-scanner. Paper 8.5 x 11 in. images of thin-sections were then used as maps to record locations of SEM backscatter images collected at magnifications of 25 to 1000X. Backscatter images were collected on two or more transects across each thin-section and labeled with orientation and location.

Computer based image analysis of SEM backscatter images was used to measure microstructural characteristics of fault zone samples and of control samples. Thirty-four SEM backscatter images from four samples were analyzed using Scion software for size and porosity (percent black and white respectively in a binary image). A cumulative size frequency plot analysis was generated for the deformation bands and control sample sands of SEM backscatter image analysis. This was accomplished by importing grain-size data from Scion Image software to Microsoft Excel. Particle long axis orientation and size (maximum diameter) were measured for each grain larger than 70 μm, and porosity was determined for each image. Image analysis results were tabulated and plotted on rose diagrams (for grain long axis orientation) or histograms (cumulative grain size distribution). Rockware statistical processing software was used to generate rose diagrams of grain orientation data gathered from Scion Image software. Kolmogorov-Smirnov (KS) statistical tests were used to compare characteristics of sample pairs.

Experimental Procedure

Experiments were carried out on control sample Alder Creek sand using a double direct shear servohydraulic testing device at the Penn State Rock Mechanics laboratory. The assembly of this apparatus encloses three rigid blocks that bound two sand sample layers that are sheared (Figure 7).

Rigid side forcing blocks with dimensions of 5 x 5 x 2 cm^3, and a center block of dimensions 10 x 5 x 3 cm^3, form the bounding surfaces shearing the material. The forcing blocks, constructed of hardened steel, maintain a constant contact area of

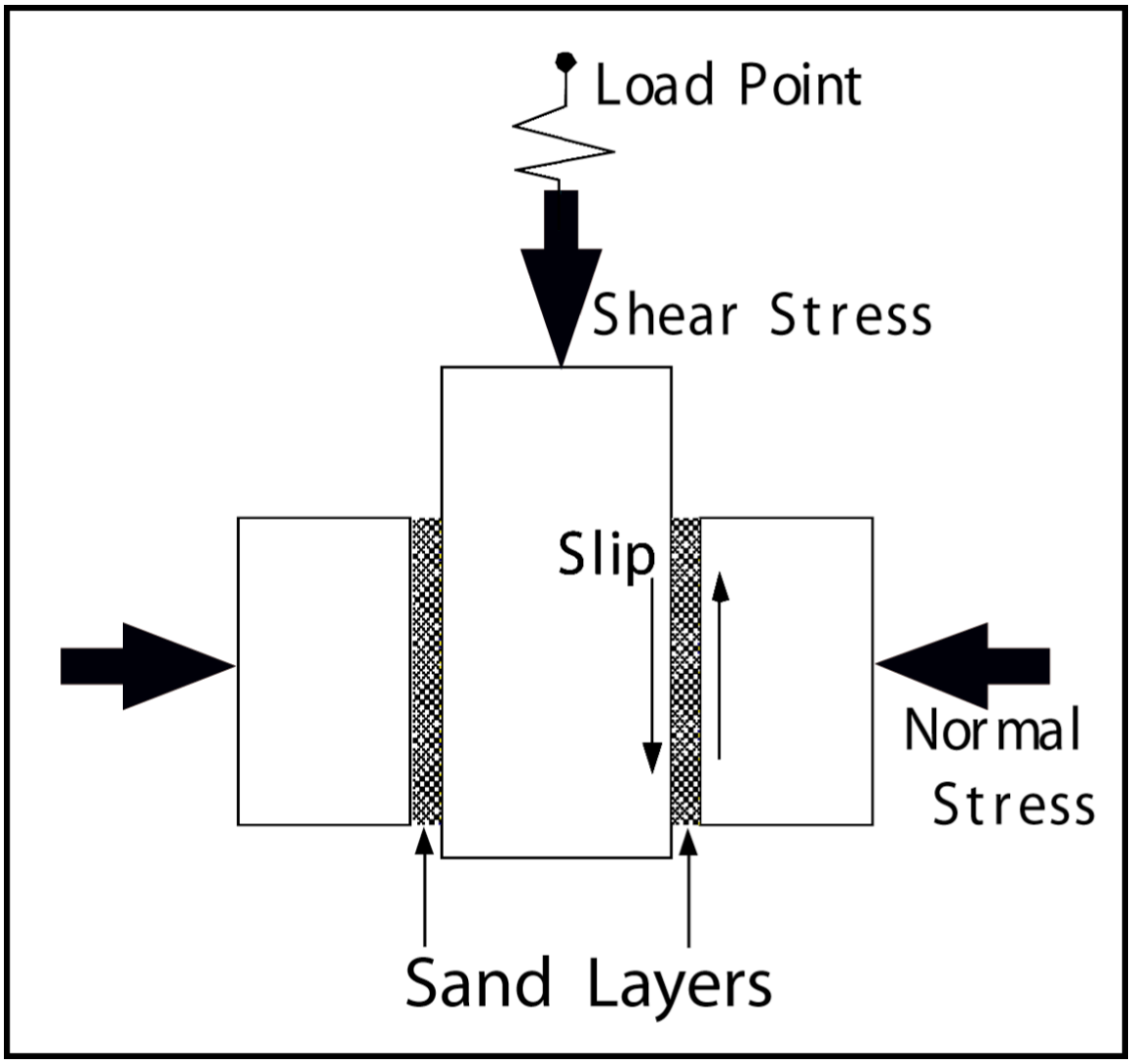

Figure 7. Diagram of the configuration of double direct shear tests. Sample sand layers (5 mm thick) are sheared between rough steel blocks. Nominal frictional contact area is 5 x 5 cm^2.

5 x 5 cm^2. Triangular grooves 0.8 mm deep with a 1.0 mm wavelength cut perpendicular to the shear sense form the roughened bounding surfaces. Construction of layers to a 5 mm thickness was done with leveling blocks and calipers. This configuration promotes localized shear development as a function of increasing net strain instead of distributed, pervasive shear. A servo-controlled load feedback mechanism with constant horizontal normal force (stress) holds the blocks in place at ± 10 KPa. A vertical servo-controlled ram forces the center block between the two stationary side blocks. Both ram's position and applied force are recorded at sampling rates between 1 and 1000 Hz, and continuously at 10 KHz.

Experiments were conducted at normal stresses of 75 to 900 KPa, a loading regime comparable to confining pressures encountered with burial depths of approximately 3 to 50 m. Shear velocities ranged from 200-2000 μm/s (2.0 to 20.0 x 10^{-6} km/s). This shear velocity is six orders of magnitude slower than coseismic surface rupture slip velocity, 3.0 km/s, observed on comparable strike-slip faults (Yagi et al., 2000). It is more than seven orders of magnitude faster than observed creep rates (Johansen and Bürgmann, 2005) of 6.4 x 10^{-13} km/s on the SAF.

Samples maintained the original moderately saturated water content from the field due to quick sample construction. All runs were conducted at a room temperature between 65-75º F.

Samples from the 100 KPa and 900 KPa experiments were preserved and analyzed for grain long axis orientation and porosity. Experimentally deformed sand sample preservation was accomplished using the same epoxy resin and hardener ratio and

method used to consolidate field samples. SEM backscatter image transects of 100, 500, and 900 KPa were then performed using a FEI Quanta 200 FEG SEM. Scion Image software was used to calculate porosity by determining percent sand grains (black) and percent pore space (white) of binary SEM images in the same method used for the Alder Creek trench control and deformation band samples. Scion Image processing software calculated orientation data and Rockware statistical software was employed to generate rose diagrams.

RESULTS

Stratigraphy and Structure in T-9 and T-10 Peel One

Bedrock

Bedrock (SAFg) at the Alder Creek site is predominately composed of Franciscan serpentinite (Baldwin, 1996). Bedrock exposed in trench T-9 is a soft, highly cohesive, dark olive-brown to dark grayish-blue, sheared "knob" of gouge containing occasional scattered, more resistant clasts. A brittle block, 15 cm thick, of oxidized bright orange to reddish-brown serpentinite caps the unit. Thin-section slide scans and SEM images of the gouge show well-foliated cataclasite (Figures 11 and 12) which most likely represents a fault zone deformed serpentinite characterized by S-C structure (Hirauchi and Hisada, 2004). I consider the S-C structure observed here to be the general Type I fabric (Davis and Reynolds, 1996). The S-surfaces appear as a horizontal foliation and banding texture whereas the thin, cross-cutting structures are the C-surfaces. In contrast, thin-sections of the brittle material capping the top of the unit show a highly weathered serpentinite with only brittle type deformation in the form of fractures.

Contacts on and within the margins of the bedrock record both deposition of young fluvial sediments from Alder Creek and multiple faulting events. The upper and western margins of the bedrock knob have been fluvially incised in a curviplanar fashion and draped with gravels (Figure 8). The eastern margin of the knob is sheared by the SAF. The fault contact consists of anastomosing vertical shears and places a sequence of

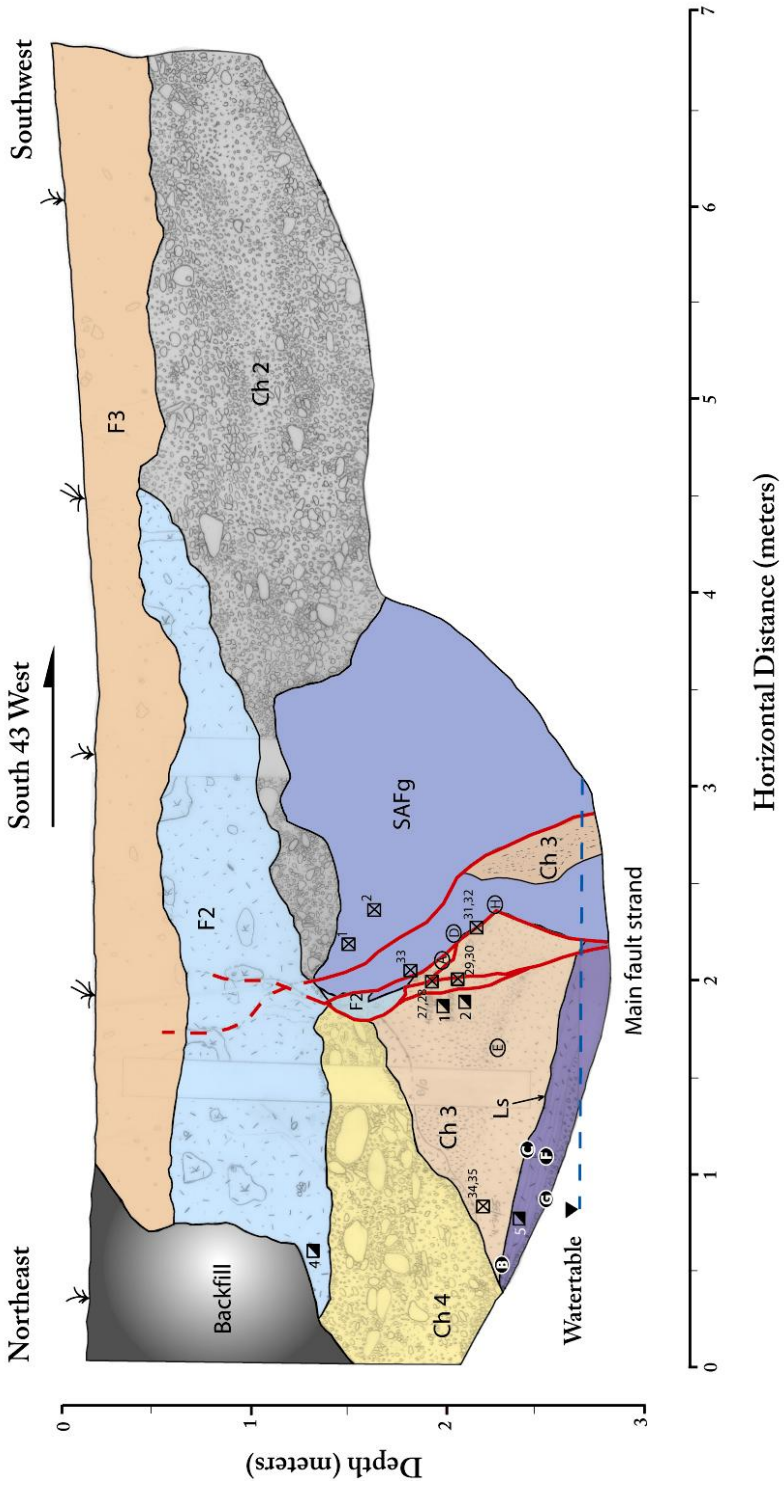

Figure 8. Log of south wall of trench T-9. See Figure 10 for explanation of units, symbols, and sample information.

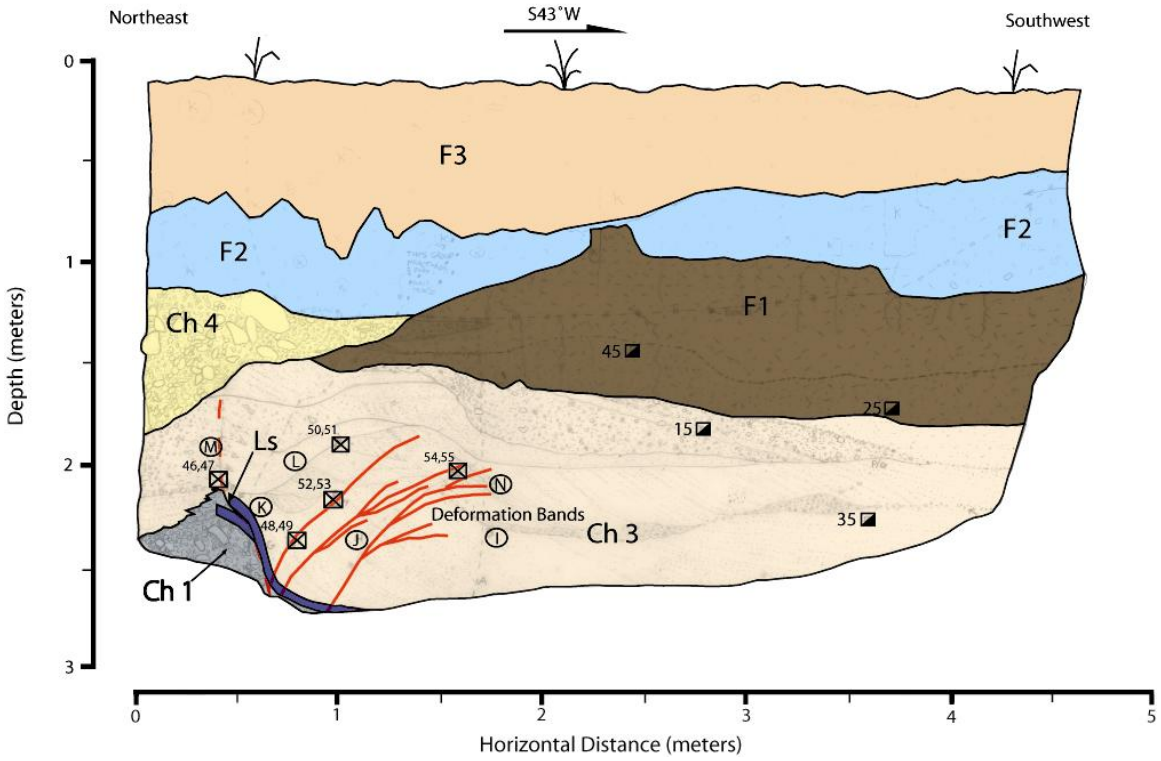

Figure 9. Log of trench T-10 Peel One. See Figure 10 for explanation of units, symbols, and sample information.

Figure 10. Geologic explanation of units, samples, including bedding and fault orientations.

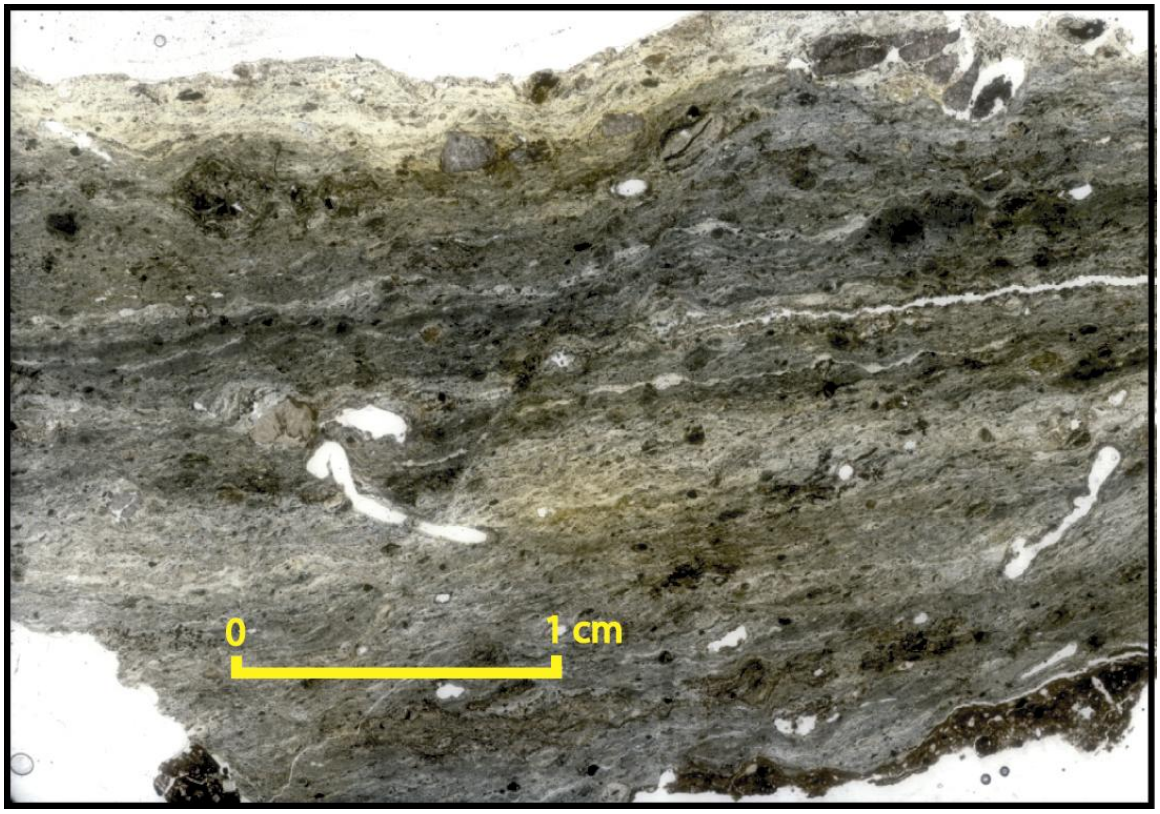

Figure 11. Slide scan of bedrock foliated serpentinite gouge from trench T-9 with 1 cm scale.

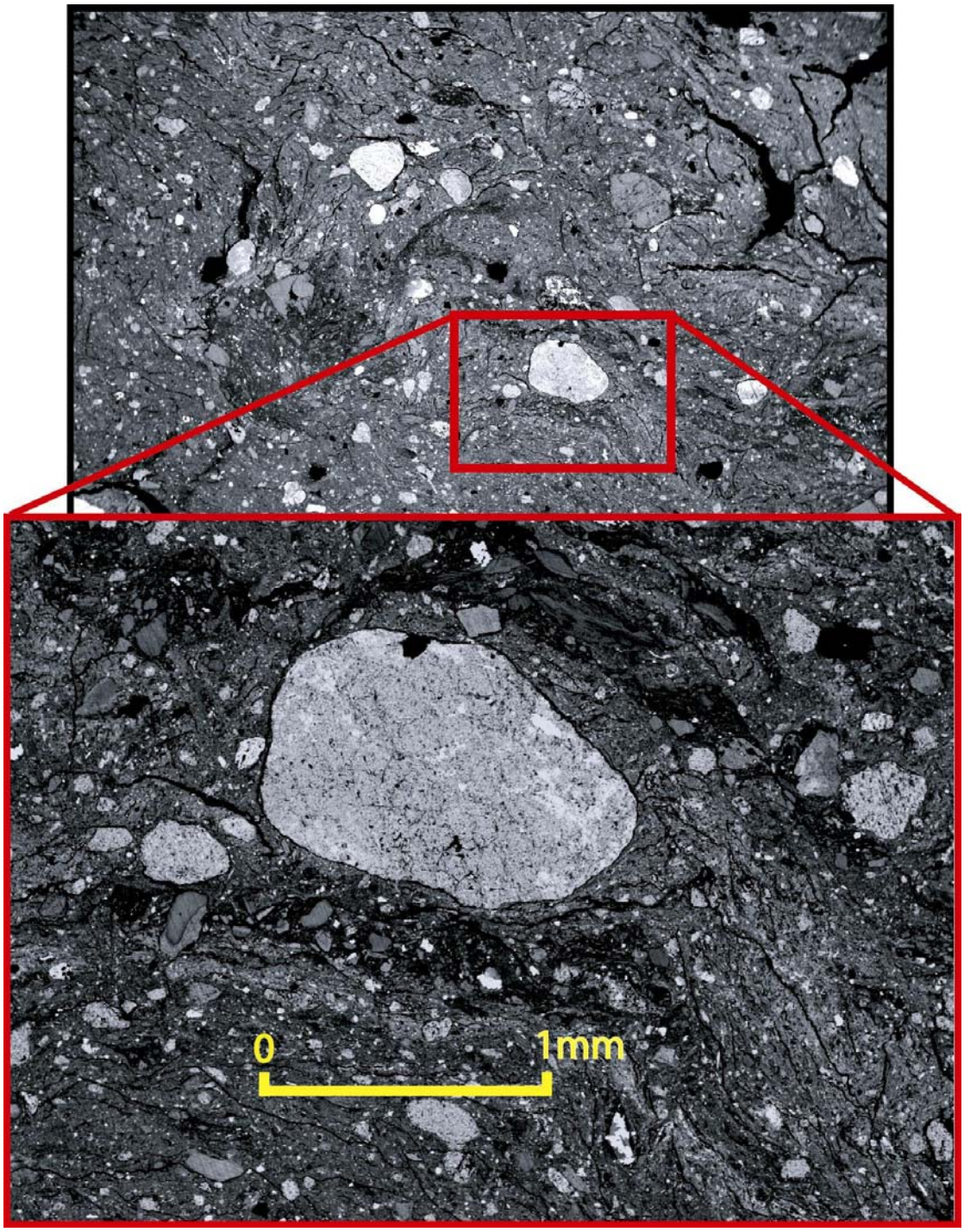

Figure 12. SEM image of foliated serpentinite gouge with 1 mm scale in enlarged image.

sand, gravel, and laminated silt deposits against the east side of the bedrock knob. An intact fault bound wedge of sand is entrained inside the lower middle section of the bedrock gouge. Scattered throughout the bedrock unit are bands of clay with silt and sand, blue-gray chert pebbles, oxidized orange-red serpentinite pebbles, and vertical bands of tan-yellow clay minerals.

Paleochannel One

Paleochannel one (Ch 1) is the oldest unit recorded previously at the site (Baldwin, 1996) and in this study is best seen at the base of Trench T-10 Peel 1 (Figure 9). It is a poorly to moderately sorted gravel and sands unit, stained reddish-brown. It is absent in T-9 but observed in T-10. Pea gravels described in this study at the basal contact with the laminated silt within this unit match those described for paleochannel unit (Ch 1) by Baldwin (1996): fine-to coarse gravels bedded to moderately sorted with manganese staining and clay films at the base of clasts. The best exposures of this channel are noted (Baldwin, 1996) to be at the southeastern most edge of the site where it unconformably overlies bedrock. The estimated age of paleochannel one (Ch 1) based on ^{14}C ages for detrital charcoal is 3045 ± 155 yr BP (Baldwin, 1996, Baldwin et al, 2002) (Table 1).

Table 1. Summary of ages of sedimentary units. The calibrated age of the laminated silt unit is based on Stuiver and Becker (1998), using CALIB software, while the interpreted age is based on the youngest or average 2 sigma (2δ) ranges. All other unit ages from Baldwin (1996) and Baldwin et al. (2005).

Sample No.	Trench	Conventional ^{14}C Age (yr BP ± 1δ)	$^{13}C/^{12}C$ (o/oo)	Calibrated Age (cal.yr BP± 2δ)	Interpreted Age-estimate
Overbank Unit (F2)					
1CS-17C	T1N	375 ± 45	-25.0	410 ±100	
16BS-20	T2S	360 ± 45	-22.3	405 ± 105	AVG <370 ± 30
Paleochannel Four (Ch 4)					
5CS-40	T1S	370 ± 60	-25.0	410 ± 110	
3CS-40	T2S	400 ± 45	-25.4	420 ± 100	
CH-1-RC-2	CRK	340 ± 40	-25.0	400 ± 100	
RC-3	T7S	410 ± 50	-25.0	420 ± 110	AVG <420 ± 20
Paleochannel Three (Ch 3)					
P1-RC2-E	T8-P1	1200 ± 40	-25.0	1120 ± 150	AVG <1120 ± 150
Laminated Silt Unit (Ls)					
T-10-RC -1N	T-10N	1100 ± 40	-22.8	1005 ± 65	
T-10-RC-2S	T-10S	1430 ± 40	-23.8	1335 ± 55	
ACT9-RC5-S	T-9S	1350 ± 40	-26.0	1270 ± 60	AVG <1230 ± 35
Paleochannel Two (Ch 2)					
22BS-54	T2S	2130± 55	-25.4	2080 ± 130	AVG <2080 ± 130
Paleochannel One (Ch 1)					
CH2-RC-1	CRK	2910 ± 40	-25.0	3045 ± 155	AVG <3045 ± 155

Laminated Silt

The laminated silt (Ls) deposit (15-25 cm thick) crops out east of the SAF at the base of T-9 (Figure 8). The silt unit consists of dark to light gray-brown finely laminated silt and very fine sand. A distinct iron oxide stained charcoal rich horizon spans the length of the unit. In T-10 (Baldwin et al, 2005) and T-10 Peel 1 (Figure 9) the silt unit crops out directly over and immediately west of the SAF. The basal contact is abrupt and irregular over reddish-orange coated pea gravels and is marked by an odoriferous layer of decomposing leaves and sticks. The unit was most likely deposited in still water near the margin of the stream channel or possibly in a small closed depression that took form following a seismic event. The laminated silt (Ls) unit could also be an abandoned channel that filled with fines during high flow events, or a deep pool abutted against bedrock that collected fines from a slow moving water column. Unit (Ls) has an estimated age, based on ^{14}C ages analysis of detrital charcoal, of 1225 ± 35 yr BP (Table 1)

Paleochannel Two

Paleochannel two (Ch 2) ranges from 0.1-1.0 m thick and is draped over bedrock west of the SAF in T-9 (Figure 8). This channel is characterized by poorly to moderately bedded, moderately sorted, clast-supported grayish-brown pea gravels and cobbles. The matrix is dark yellowish-brown with light yellow mottling. Much of the material in this channel is stained with a reddish-brown manganese oxide. There is a poorly to moderately developed clay film at the gravel base. A 10-15 cm thick, yellowish-brown layer of coarse sand and pebbles spans the middle of the unit. The majority of unit (Ch 2)

I interpret to represent relatively high energy flow where the Alder Creek thalweg scoured and filled bedrock. The estimated age of this unit based on ^{14}C ages for detrital charcoal is 2080 ± 130 yr BP (Table 1).

Paleochannel Three

Paleochannel three (Ch 3) is a 1 m thick, moderately to well bedded, yellowish to reddish-brown, laminated fine-grained to coarse-grained sandy unit that overlies the laminated silt unit east of the SAF in T-9 (Figure 8). In contrast, in T-10 Peel 1, the unit is present on both sides of the fault. Here it is folded and tilted with dips ranging from 21-70º SW. The basal contact with the Ls unit is irregular to gradational. The upper and eastern margin is wavy and irregular with a thin 1-5 cm thick strip of yellowish-brown coarse sandy silt and clean scattered pebbles. This strip may represent a remnant overbank deposit eroded by the overlying unit (Ch 4) gravels. The upper western margin is in abrupt fault contact with bedrock (SAFg) (Figure 8). Unit (Ch 3) was probably a bank deposit or small point bar within a turn or meander of Alder Creek. Much of the unit is truncated due to erosion of the overlying paleochannel deposit (Ch 4) and from fault truncation. The estimated age for this unit, based on ^{14}C ages for detrital charcoal, is 1240 ± 105 yr BP (Table 1).

Overbank Deposit One

This unit is only seen in T-10 peel 1 (Figure 9) of this study. The unit ranges from 0.5-0.75 m in thickness. It undulates and is erosionally pinched out to the east by the overlying paleochannel unit (Ch 4). The lower section of this unit overlies deposit (Ch 3). It is light yellowish-brown, massive to faintly laminated, silty fine-grained sand

with abundant charcoal flecks. Overbank unit (F1) might represent an older flood overbank deposit or the edge of an alluvial flat associated with the development of a meander in the creek. The uppermost portion of this unit is a dark yellowish-brown buried soil (paleosol) consisting of silt and fine sand that break apart into small poreless peds and clods. The degree of pedogenesis suggests that this portion of the creek bank may have had a relatively long quiescent period possibly due to a drastic fluvial change or tectonic uplift. The age of the overbank deposit (F1) is currently unknown. Its stratigraphic position indicates that it is younger than 1240 yr BP (unit Ch 3) and older than 400 ± 100 yr BP (unit Ch 4).

Paleochannel Four

This unit ranges from 0.25-1.0 m in thickness and consists of large (up to 35cm) gray to olive-brown cobbles and gravels in a yellowish-brown silt and coarse sandy matrix. This paleochannel unit (Ch 4) is coarsely bedded and sorted, and contains the slightest veneer of clay film under clasts. The western margin is in abrupt fault contact with colluvium associated with overbank unit (F1). The middle and eastern margin's basal contact is curviplanar and abrupt with paleochannel unit (Ch 3) and the silt unit (Ls). This paleochannel unit (Ch 4) reasonably represents an in-channel or thalweg deposit due to the large, coarse material composition and the extent of erosion of the underlying materials. The maximum age of the unit is 400 ± 100 yr BP based on ^{14}C ages from detrital charcoal (Table 1).

Overbank Deposit Two

This 0.75-0.25 m thick older overbank deposit is light olive-brown to light yellowish-brown predominantly silt with medium and coarse-grained sands. Charcoal chips and flecks are peppered throughout the unit. There is heavy bioturbation in the form of krotovinas, pervasive insect tunneling, and roots. The upper contact of the unit is obscured in various places with the younger overbanks unit (F3). In trench T-9, overbank unit (F2) overlies paleochannel unit (Ch 4), east of the SAF, and paleochannel unit (Ch 2), west of the SAF, along an irregular contact. Also observed in trench T-9 directly on the main trace of SAF, overbank unit (F2) has a fault-derived colluvial wedge that has been juxtaposed between bedrock and paleochannel units (Ch 3) and (Ch 4). Overbank unit (F2) was likely created by annual bankful and flood events from a bend in Alder Creek that has lightly scoured underlying units and deposited charcoal, detritus, suspended silts, and sands. The maximum calibrated age for the unit based on ^{14}C ages from detrital charcoal is about the same as the underlying paleochannel four (Ch 4) at 400 ± 90 yr BP (Table 1).

Overbank Deposits Three

The youngest unit exposed in both trenches T-9 and T-10 Peel 1 is overbank unit (F3). This 0.30-0.60 m thick silty unit has been extensively bioturbated from plowing, previous fault trenching, gopher holes, and plant roots. It contains minor amounts of fine sand and scattered pebbles. The olive-brown organic horizon is faint and dry with common pores, common roots, and angular and pocked peds 0.5-2.0 cm wide. Although

the present altered state of overbank deposit (F3) has obscured parts of the basal contact with overbank deposit (F2), the contact undulates where undisturbed.

Structure

The active trace of the SAF juxtaposes an “anomalous buried bedrock high” (Baldwin, 1996) on the west with fluvial sediments on the east. Faulting in bedrock is exhibited in the eastern margin as discrete, anastomosing shears. The bedrock’s northeastern 0.25 m edge, margin, and abutted sediments have been repeatedly sheared with a slight apparent east side down vertical displacement in trench T-9.

The active trace of the SAF is best exposed in trench T-9 (Figure 8) as a narrow, anastomosing fault zone about 1.2 m wide that terminates 0.4 m from the surface. The fault strikes N25ºW to N31ºW and dips steeply (64-81°) southwest. Trench T-10 Peel 1 exposes a set of branching east dipping faults on the west side of the SAF. The trench’s base reveals a fault that strikes N36ºW that dips from 90º to 85ºSW. It ruptures paleochannel unit (Ch 1) gravel up through the silt unit (Ls). The silt unit (Ls) is nearly horizontal at the unit’s western edge; at the eastern margin of the trench it is openly folded, is monoclinal, buckled, and shortened with a 20 cm section repeated on top of itself (Figure 9). In gravels, the faults are unrecognizable except for conspicuous zones of vertically rotated clasts in areas where fluvial imbrication is present. In the silt unit (Ls) of trench T-10 Peel 1, the fault was observed as a distinct light colored shear.

The SAF zone in paleochannel unit (Ch 3) consists of both faults and deformation bands. Deformation bands are primary faulting structures that occur in porous

sandstones. Deformation bands have displacements on the millimeter to centimeter scale, and have smaller grain-size, poorer sorting, and lower porosity than the original parent material (Aydin, 1978). They are more resistant to erosion than surrounding sand due to loss of porosity and increased cementation (Davis and Reynolds, 1996). To the naked eye, the deformation bands are characterized by slightly offset laminations and have a lighter color, finer texture. The deformation bands found in the paleochannel unit (Ch 3) sands of trench T-9 are steeply dipping to vertical, anastomosing, discrete shear zones, 2-10 mm thick. They physically change (invisible or non-existent) where they extend into the coarser or finer grained units above and below. In T-10 Peel 1, deformation band structures form prominent parallel to sub-parallel branches 5-20 cm apart. They offset sand laminations east side up 1-2 cm, are 5-10 mm thick, strike N14ºW and dip 55ºNE.

Microstructure of the Fault

Deformation bands from paleochannel unit (Ch 3) sands were sampled in trench T-9 for microstructural analysis and characterization. Two representative sample pairs, control samples (CS-34-35) and fault samples (FS-27-28), were chosen from within and outside the fault zone.

The control samples, as seen in thin-section, slide-scan and SEM images, are clean and loosely packed with a relatively homogenous distribution of pore space (Figure 13).

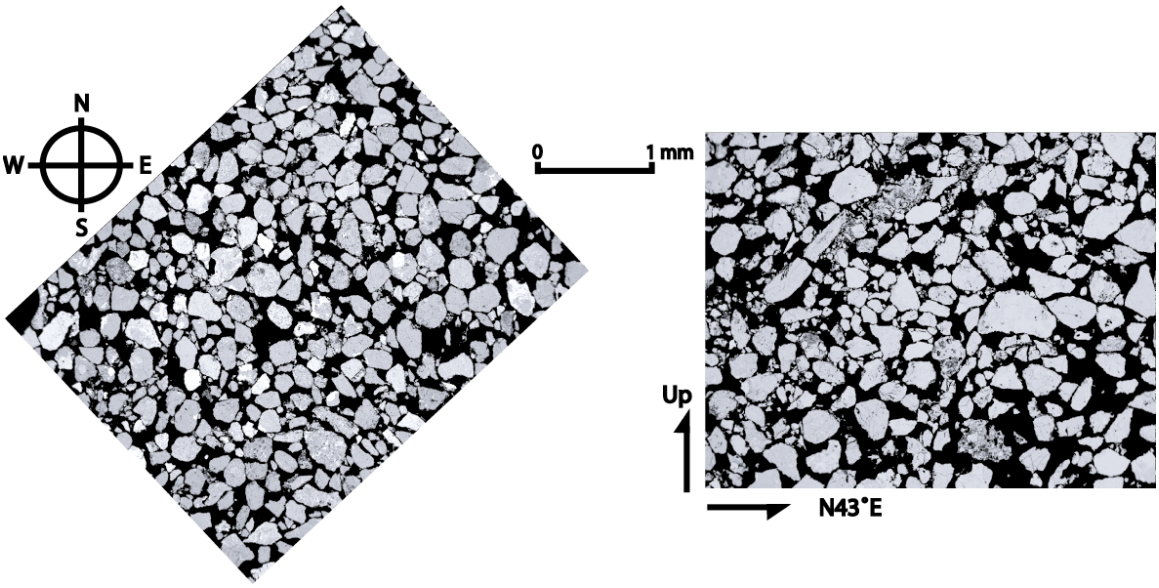

Figure 13. SEM images of control horizontal sample 4-35 (left) and vertical sample 4-34 (right). 1mm scale bar is for both images.

Sand grains are almost entirely intact, and have a limited size range (predominantly fine sand). Sand grains show a preferred orientation, are well sorted, and have grain shapes that are sub-angular to sub-rounded. Ultra-thin clay coatings bridge spaces between sand grains. Preservation of these delicate clay bridges shows that grain-to-grain contacts were not disturbed during sample collection or thin-section preparation.

Sand is a mix of mostly lithic grains, with smaller amounts of quartz, feldspars, and minor amounts of altered volcanic glass and detrital charcoal fragments. Grain composition was determined with 100 point counts on two separate control sample thin-sections using a petrographic microscope. Composition, divided into four categories,

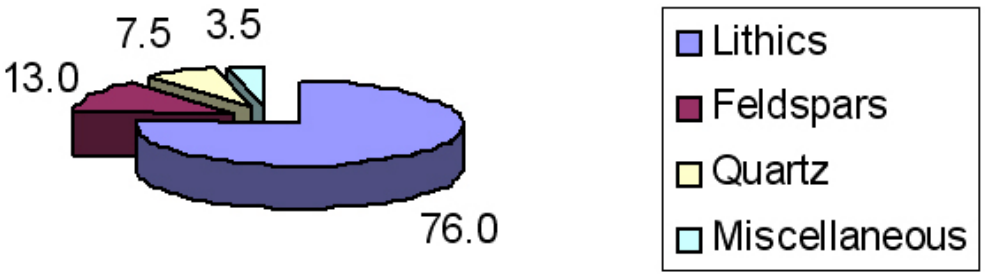

Figure 14. Pie chart representing the percent of each composition category.

include: lithics 76%, feldspars 13%, quartz 7.5%, and miscellaneous 3.5%, comprised of altered glass, clay, and charcoal (Figure 14).

In contrast, sands within the deformation bands, as seen in thin-section, slide-scan, and SEM images, are more tightly packed and have variable pore space. Pore space within the band is reduced compared to the pore space of sand immediately outside the deformation band and within control samples (Figure 15).

The sample pairs, horizontal (map view) and vertical (trench wall view) representatives, were quantitatively analyzed for cumulative size distribution (~70 µm to ~ 1 mm), grain long axis orientation (trend in the horizontal view and plunge in the vertical view), porosity, and lithological composition. The sand grains lie within the very-fine to coarse sand classification after the Wentworth scale (Prothero, 1996).

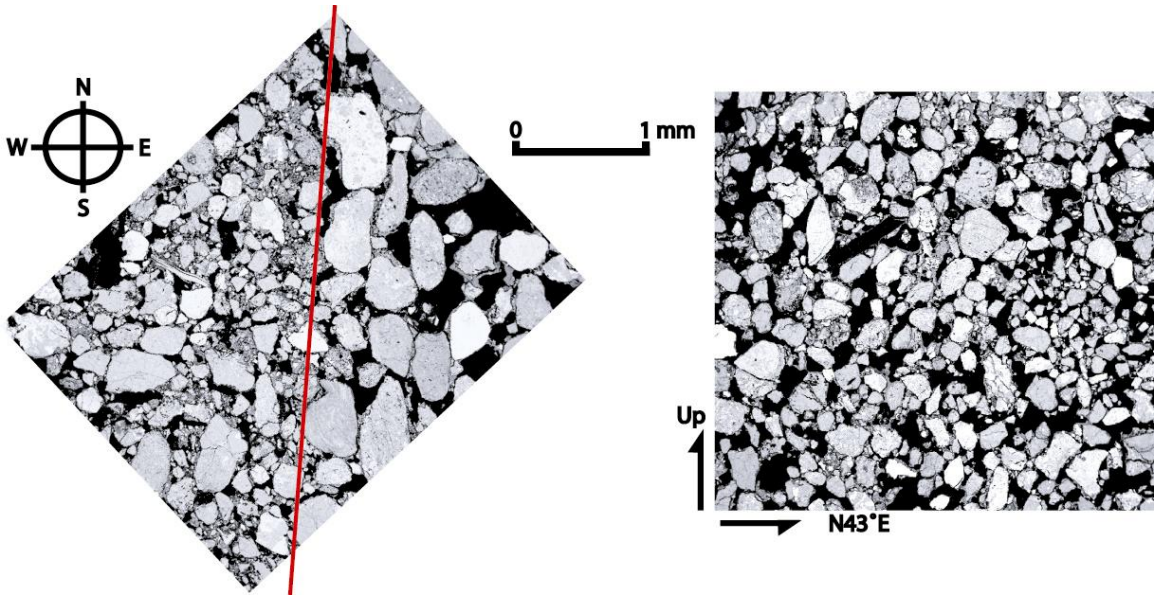

Figure 15. SEM images of deformation band horizontal (map view) sample 4-28 (left) and vertical (trench wall) sample 4-27 (right). 1mm scale bar is for both images. The red line indicates the approximate deformation band boundary in sample 4-28 with undeformed sand at right and deformation band at left.

The deformation band sands are more fine-grained than sands in control samples. (Figure 16). Grain-size in deformation bands is 30-33% fine-grained sand with 18-20% medium-grained sand, while the control sample has 16-17% fine-grained sand and 31-37% medium-grained sand.

Control and deformation band samples have long axis particle positions that indicate moderate to strong preferential orientations. A rose diagram for horizontal control sample 4-35 shows sand grains strongly clustered around a N40-70ºE trend, while the vertical rose diagram for control sample 4-34 shows grains plunging 20-40ºSW

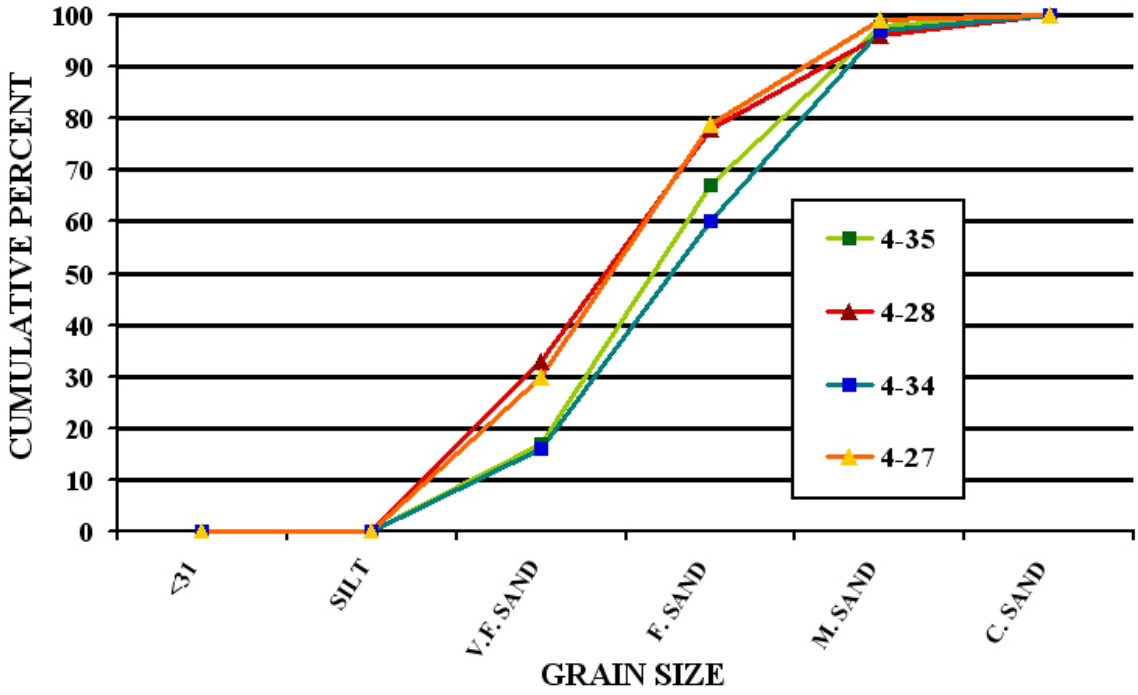

Figure 16. Cumulative grain-size distribution for sand inside deformation bands (4-27, 4-28), and for control sample sand greater than one meter away from the fault (4-34, 4-35).

(Figure 17). The horizontal deformation band (sample 4-28) rose diagram indicates two distinct orientations, one trending N10-20E, and the other almost due East-West. The rose diagram for the vertical sample, 4-27, indicates grains have a vertical long axis orientation 30º viewed in the NE-SW direction (Figure 18).

Kolmogorov-Smirnov (KS test) statistical comparisons of sand grain orientations within deformation bands to orientations in control samples, were used to determine whether these two probability distributions differ (Table 2). The probability distribution

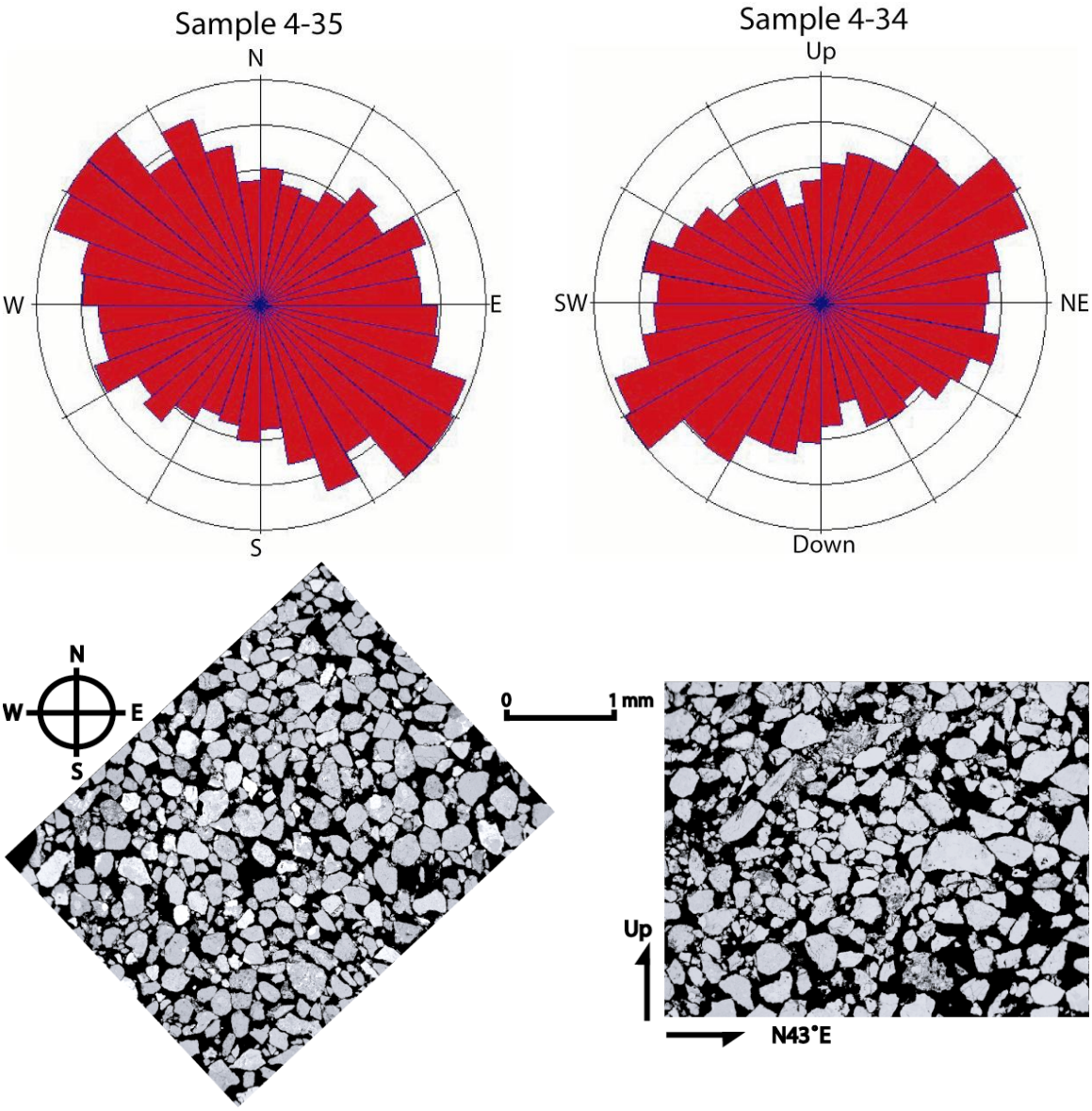

Figure 17. Rose diagrams of sand grain orientation from control samples. Rose petals represent relative number of grains found within each 10º increment. Capitol letters N, S, E, W, NE, and SW represent azimuth directions. Number of grains analyzed in 4-35 are n =3255, and in 4-34 n =2465. SEM images of control horizontal (map view) sample 4-35 (left) and vertical (trench wall view) sample 4-34 (right). 1mm scale bar is for both images.

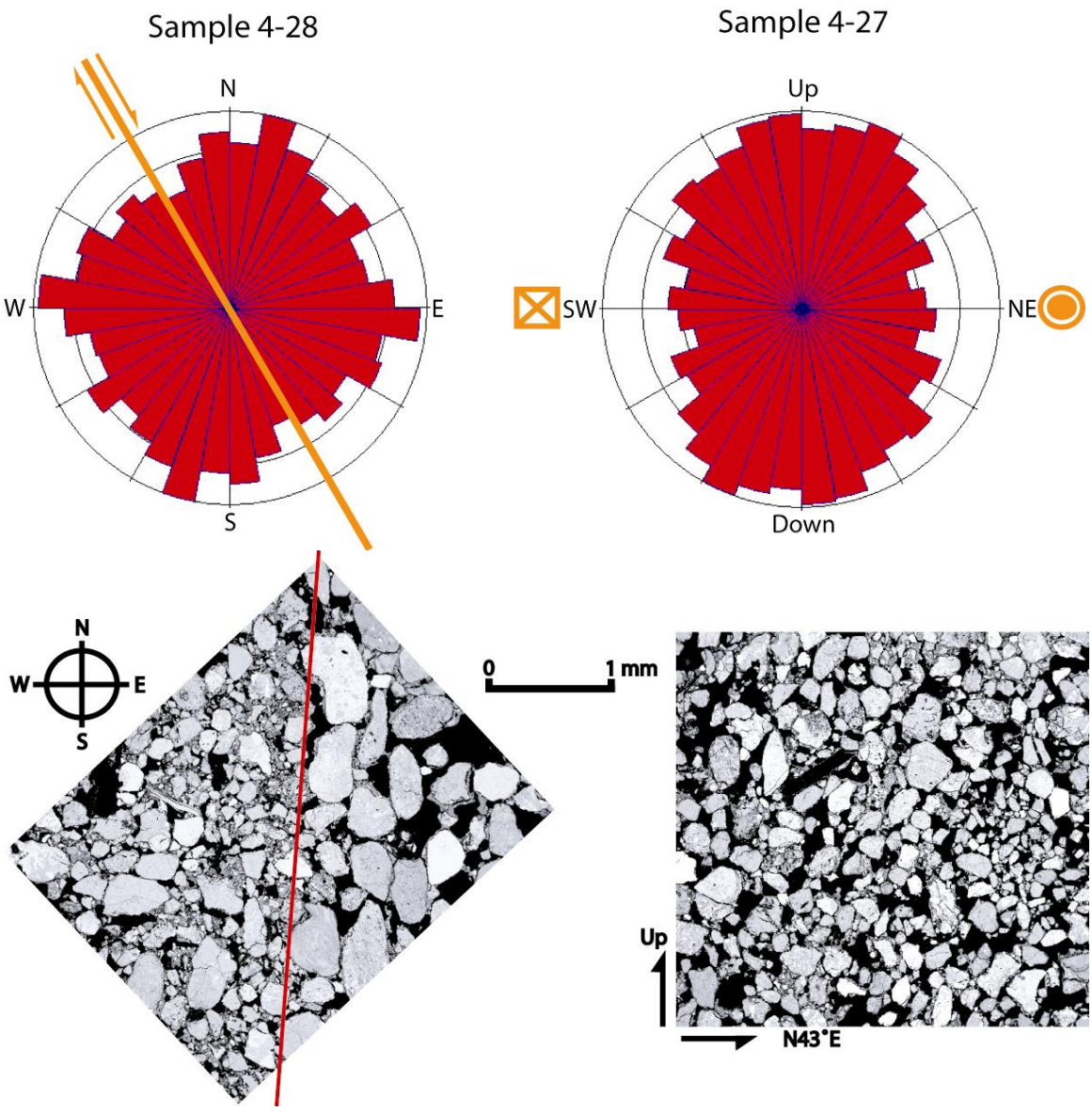

Figure 18. Rose diagrams of sand grain orientation in deformation bands. Letters have the same significance as Figure 17. SAF orientation (N30ºW) with right lateral shear sense shown for reference in the horizontal sample 4-28. The box with an X (into the page) and the circles (out of the page) represent SAF shear sense in the vertical 4-27 sample. The number of grains analyzed in 4-28 are n =2839, and in 4-27 n =3160. SEM images of deformation band horizontal sample 4-28 (left) and vertical sample 4-27 (right). 1mm scale bar is for both images. The red line indicates the approximate deformation band boundary in sample 4-28 with undeformed sand at right and deformation band at left.

here is defined as all the values, between 0˚ and 180˚, that the variable (grain orientation) can possibly take and the likelihood that each would occur. The two-sample KS test provides a general nonparametric method for comparing two samples because it is sensitive to differences in both location and shape of the empirical cumulative distribution functions of the two samples (Kirkman, 1996). In this case, I use it to test the null hypothesis that the unfaulted and faulted grain orientation distributions are the same. The KS test P-value (the P-value is the probability of getting a test statistic this extreme if the populations are the same) indicates that the grain orientation distributions of fault samples and control samples are statistically different (Table 2).

Table 2. Kolmogorov-Smirnov test results

	Samples to be tested	P-Value
Horizontal	Control 4-35 vs. Deformation Band 4-28	<0.0001
Vertical	Control 4-34 vs. Deformation Band 4-27	<0.0001

Porosity was determined in control samples and deformation band samples by analyzing SEM images (Table 3). Control samples have a combined average porosity of 38.5 ± 2.4%, whereas the combined porosity inside the deformation band is 22.8 ± 3.5%. These porosity measurements show that at least 10% porosity reduction accompanied the formation of deformation bands.

Table 3. Control and deformation band sample porosity results.

	Sample	Ave. Porosity ± 1 Standard Deviation	Images Analyzed (n)
Vertical	Deformation Band 4-27	22.5 ± 3.1	6
Horizontal	Deformation Band 4-28	23.1 ± 4.1	6
Vertical	Control 4-34	39.7 ± 2.1	8
Horizontal	Control 4-35	37.3 ± 2.2	10

Rock Mechanics

As a preliminary study of the basic frictional properties of the Alder Creek sands, I brought unfaulted sand samples to the Pennsylvania State University Rock Mechanics laboratory and used a double direct shear testing apparatus to address two questions:

How do deformation bands form in young near-surface sediments? Previous studies of porous, quartz-rich sandstones in the southwest document formation of deformation bands in well-lithified units, i.e., in conditions of moderately high confining pressure (Antonellini and Aydin, 1994). Confining pressure is a function of material density and burial depth. However, experimental studies conducted on poorly-lithified or unlithified sediments under low confining pressures, like those at Alder Creek, suggest that deformation bands are not expected to form under these conditions.

If wet sand ranges from 1900-2500 kg/m^3 then burial of sand 3 m deep would generate a confining pressure of approximately 55-75 KPa, and sand buried 100 m deep

would equate to 1.8-2.4 MPa. Angular quartz gouge experimentally sheared at a confining pressure of 5 MPa corresponding to ~200-275 m burial has been shown to lack grain fracture and have homogeneous texture until stresses upwards of approximately 50 MPa (~2-2.75 km burial) were obtained (Mair et al., 2002a). Experimental deformation band formation in porous, quartz rich sandstone is "strongly sensitive" to confining pressure occurring only at 13.5-54.8 MPa or ~0.5-3 km burial depth (Mair et al., 2002a). These observations suggest that deformation bands are not expected to form at or near the surface.

The second question is, does this material exhibit velocity strengthening behavior? Materials within deformation bands of porous, quartz-rich sandstone appear to undergo strain hardening as a result of the deformation (Aydin, 1978). If the material's strength increases during simple shear then strain might be redistributed laterally into adjacent weaker, unfaulted materials.

In order to address these questions I ran a series of simple shear experiments on Alder Creek sand layers. I used a computer-regulated displacement record while maintaining confining pressures ranging from 75 to 900 ± 10 KPa. The range of normal stress was chosen as an analog for a burial of approximately 3-45 m deep. The additional controlling variable considered for these experiments are sliding velocity (ranging from 10-2000 μm/s). The friction parameters I measured were: the coefficient of sliding friction (μ), the a-b parameter, shear stress vs. shear displacement, and the angle of internal friction.

In all experimental runs, a peak value of shear stress was reached followed by a small period of weakening, which was then followed by a relative steady-state frictional equilibrium. Velocity steps were run to assess second-order changes of frictional properties following initial constant driving velocities. The history of loading for all runs consisted of an initial rate of 20 μm/s followed by step changes of 200 μm/s at 6 mm displacement. At 12 mm displacement the velocity step changes were increased to 2000 μm/s. A cumulative displacement of 25 mm was reached for each example.

The coefficient of kinetic friction (μ), is a dimensionless quantity derived from the kinetic friction force (referred to here as the residual shear stress) between two sliding surfaces divided by the normal force (referred to here as normal stress or confining pressure). The average measured steady-state coefficient of sliding friction μ, is calculated from each residual shear stress point divided by a corresponding normal stress. Values range from 0.41 to 0.54 with an average of 0.47 ±0.04 (Table 4). A regression of the residual shear stress vs. normal stress suggests a nearly linear relation between the two parameters. It suggests a slightly higher μ value of 0.51 (Figure 19).

The friction rate parameter (a-b) is a measurement of the changes in friction with respect to shear velocity (velocity changes or “steps” generally an order of magnitude at a time). These (a-b) values are typically small and dimensionless (0.001-0.1), yet define whether materials have the capability to host stable slip (values > 0) or

Table 4. Coefficient of friction results for each experiment, 75 to 900 KPa normal stress where the average Coefficient of Friction (μ) ± 1 Std Dev = 0.47 ± 0.04.

	75 KPa Exp.	100 KPa Exp.	200 KPa Exp.	300 KPa Exp.	400 KPa Exp.	500 KPa Exp	550 KPa Exp	900 KPa Exp
Residual Shear Stress (KPa)	33.3	51.9	94.5	132.8	165.4	227.4	263.1	473.4
Avg. Normal Stress (KPa)	76.8	97.0	199.9	303.0	402.0	505.0	541.0	911.4
Friction (μ)	0.43	0.54	0.47	0.44	0.41	0.45	0.48	0.52

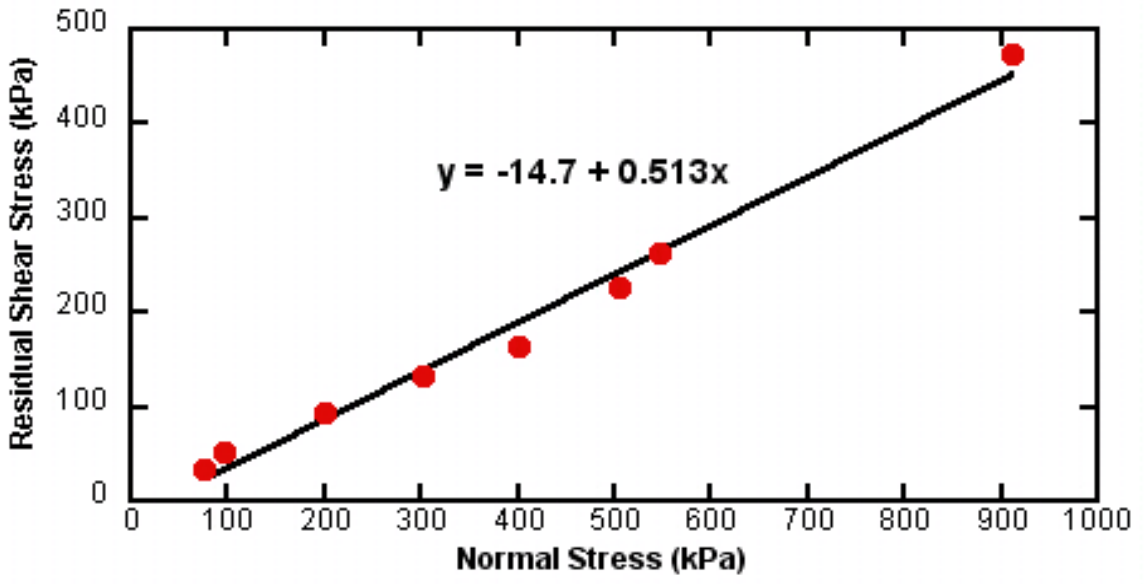

Figure 19. Residual shear stress is plotted as a function of normal stress. The equation represents the linear regression of the data. The angle of internal friction (~27º) is derived from the angle between the normal stress axis and the line.

unstable slip (values < 0) (Marone, 2006, person. com.). Figure 20 illustrates this small change in friction following a velocity step on the 900 KPa experiment. The term "a" refers to the total increase in friction immediately following a velocity jump. The term "b" is the value of total frictional decrease to a new steady state following the velocity jump. The a-b values were relatively high (0.11) at the lowest confining pressures and steadily decreased to very low values (0.005) at the highest confining pressures (Figure 21).

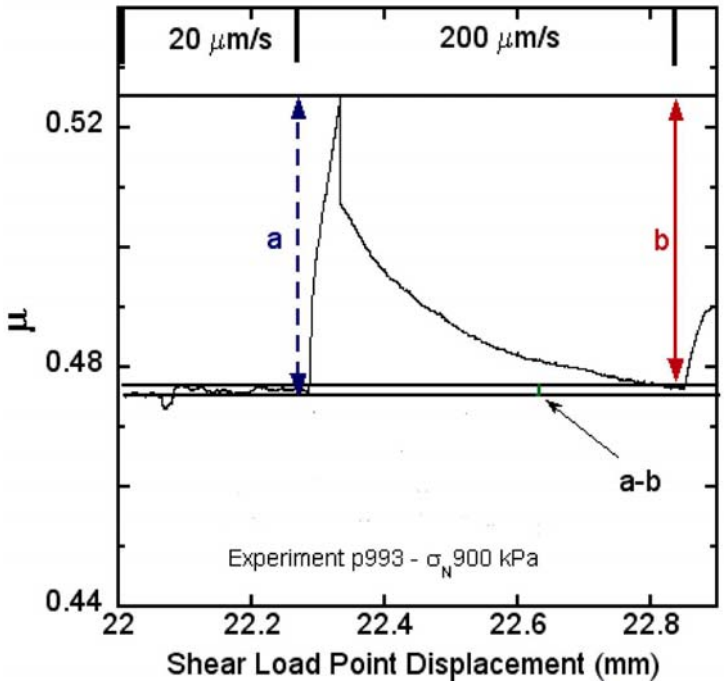

Figure 20. The coefficient of friction (μ) plotted as a function of shear displacement (mm). Velocity steps reveal the a-b parameter (second-order changes).

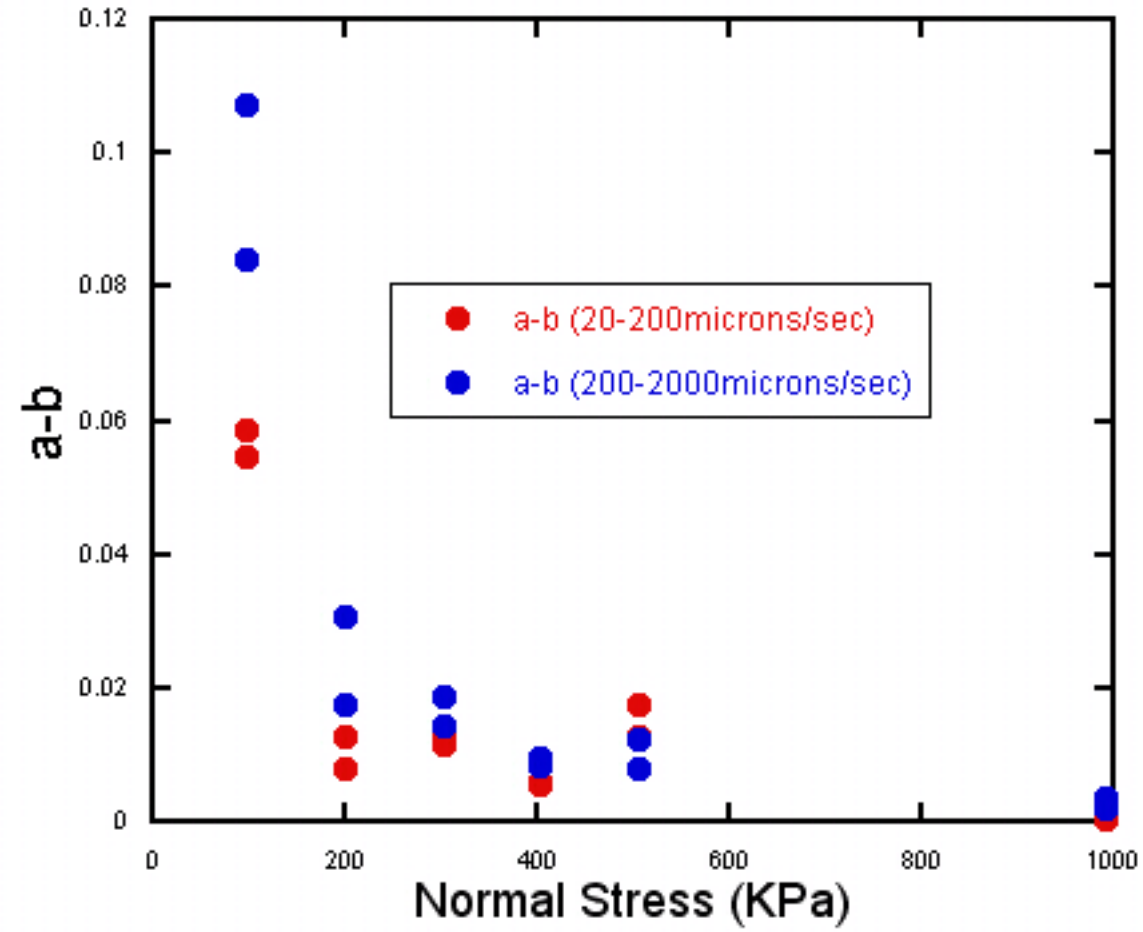

Figure 21. The a-b parameter is plotted as a function of normal stress for velocity jumps 20-200 µ/s (red dots) and 200-2000 µ/s (blue dots). Note that the value of a-b is small compared to overall friction and approaches zero at 900 KPa.

A plot of shear stress vs. shear displacement is useful in determining whether compaction or stable/unstable sliding occur during the experiment (Figure 22). Experiments show that when quartz sand layers contain less than 30% angular particles, and constant velocities are applied, unstable sliding (erratic jumps in shear stress during displacement) occurs (Anthony and Marone, 2005).

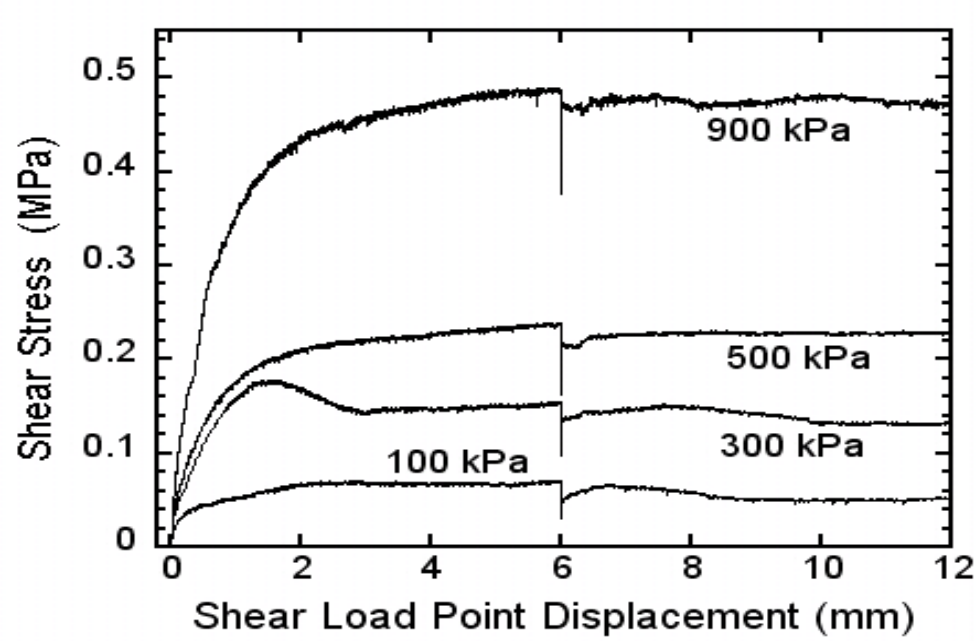

Figure 22. Shear stress (MPa) plotted as a function of shear displacement (mm) for experimentally sheared sands at all normal stress conditions (KPa). Note the velocity jump (programmed for the arbitrary point) at 6 mm displacement, there is a slight decrease (compaction) and steady values (stable sliding) of shear stress during displacement for the 100, 300, and 500 KPa samples.

In my experiments on Alder Creek sands, a shear stress maximum was followed by a small period of weakening (<1 mm displacement) before attaining a relative steady-state frictional equilibrium (Figure 22). In the simple shear experiments, Alder Creek sand samples exhibited stable slip, consistent with sub-angular to sub-rounded shapes of the sand grains (Anthony and Marone, 2005).

The angle of internal friction for Alder Creek sand was determined by plotting the residual shear stress (steady-state shear stress after several mm of displacement) with respect to normal stress values. Linear regression of these data represents a failure

envelope (tangent line to circles of critical stress states). The slope of the regression line defines the internal friction angle. The measured angle was 27.2º.

Another result of the experiments was that observed porosity was greatly reduced with increased confining pressure. For example, porosity of the 100 KPa and 900 KPa samples was, on average, 30.3 ± 1.4%, and 8.9 ± 3.5% respectively (See Table 5).

Table 5. Porosity results for 100 KPa and 900 KPa experiments.

Sample	Ave. Porosity ± 1 Standard Deviation	Images Analyzed (n)
100 KPa	30.3 ± 1.4	7
900 KPa	8.9 ± 3.5	10

Preferred grain orientations in the 100 KPa sample is 30-50º counter-clockwise from the shear zone, with a small population clustered at 0-20º clockwise (Figure 23a). At 900 KPa, grains show a strong preferred orientation from 20º clockwise to 10º counter-clockwise from the shear zone, with a small population also occurring 20-70º counter-clockwise from the shear direction (Figure 23b). These results imply that there is a complex relationship between confining pressure, shear, and microstructures of experimentally deformed sand samples.

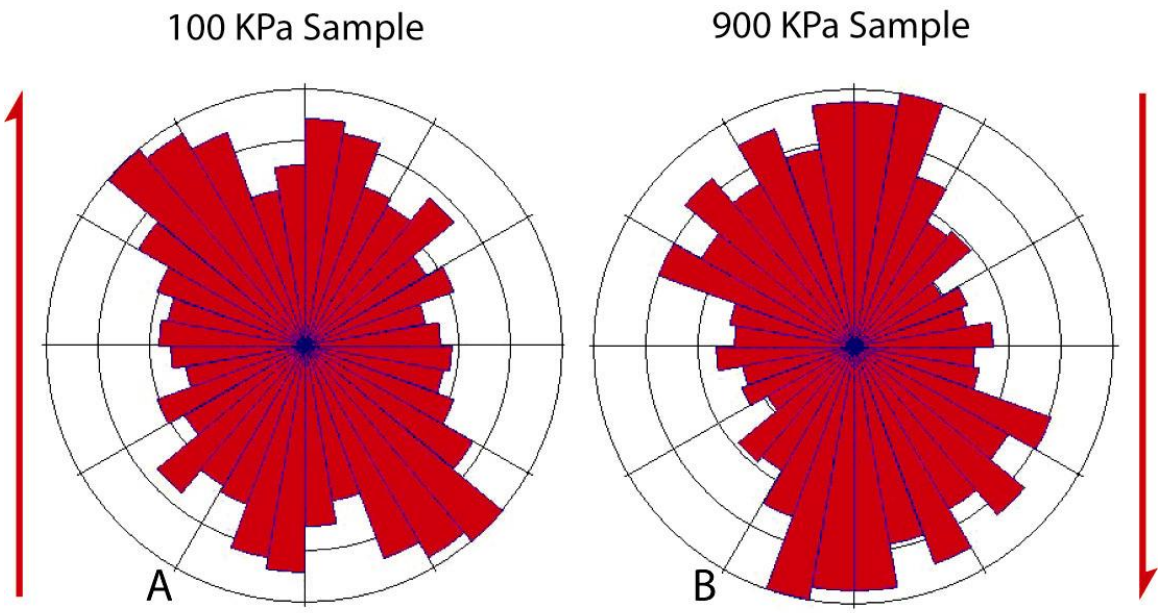

Figure 23. Rose diagrams of experimentally sheared Alder Creek sand normal stress end-members a) 100 KPa and b) 900 KPa. Arrows indicate the sense of shear from the experiments. Rose petals represent relative number of grains found within each 10º increment. Number of grains (n) analyzed in the 100 KPa sample are 533, and in the 900 KPa, n = 504.

DISCUSSION

Paleoseismic Interpretation

Based on evidence from regional paleoearthquake data and on stratigraphic and structural characteristics of this (T-9, T-10 Peel 1) and previous studies (Table 1), Alder Creek fluvial sediments record at least three coseismic slip events since AD 690 (Baldwin, 1996; Baldwin et al., 2005). The maximum limiting age, AD 690, is derived from the laminated silt unit (Ls) that occurs at the base of trench T-9 and Peel 1 from T-10 (Figures 8 and 9).

The most recent fault strand, rupture Z, shears through bedrock, overbank unit (F2), and terminates diffusely into the youngest unit, overbank unit (F3), about 0.4 m from the surface (Figure 24). The fault strikes N29ºW and dips from 60°SW to nearly vertical. The uppermost portion of the shear has a notable chalky white color that is distinct from the yellow color of the overbank fines (F3). I interpret this to represent the 1906 surface rupture that does not extend to the surface due to disturbance by plowing and bioturbation.

The second oldest (penultimate) rupture, Y, is a meandering shear, sub-parallel to the 1906 rupture. This fault bounds the northeastern edge of bedrock (SAFg). It transects the lowermost silt unit (Ls) and paleochannel unit (Ch 3), and terminates diffusely into the older overbank unit (F2) (Figure 24). A fault derived colluvial wedge from overbank unit (F2) is juxtaposed between the bedrock margin shear and the paleochannel unit (Ch 4).

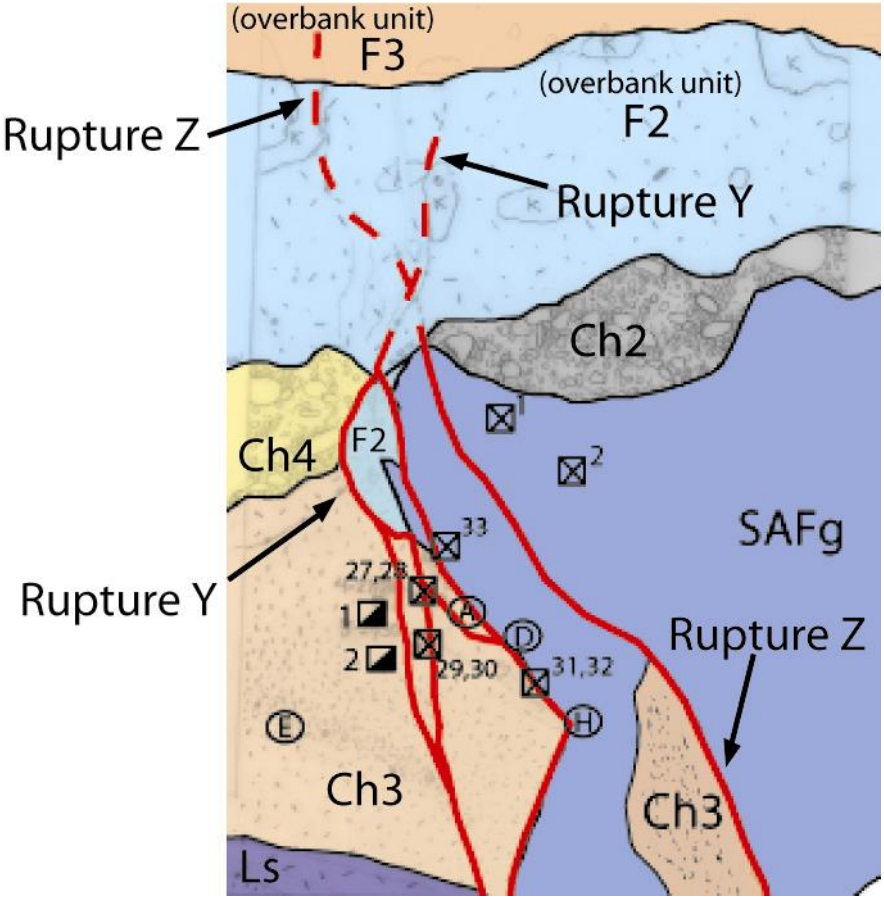

Figure 24. T-9 close up of fault zone with locations of ruptures Y and Z. Stratigraphic units and sample location explanations from Figure 10.

Charcoal within the overbank unit (F2) (AD 1440-1640, Baldwin, 1996), provides a maximum limiting age of AD 1640 for this rupture.

An angular unconformity (exposed in trench T-9 and T-10 Peel 1, Figures 8 and 9) between the laminated silt unit and the overlying paleochannel unit (Ch 3) sand provides evidence for a third surface rupture event. The evidence occurs in trench T-9 where bedding in the laminated silt unit strikes N7° E and dips 15° NW, while the foreset

beds of the overlying paleochannel unit (Ch 3) sand at the contact strike N12°W to N24°W and dip up to 31° SW. Additionally in T-10 Peel 1, bedding of the laminated silt unit (Ls) strike N70ºW and dips from 45-70º SW, while the foreset beds of the overlying paleochannel unit (Ch 3) strike N38°W to N81°W and dip from 21-40°SW. The laminated silt unit (Ls), age AD 690-760, was deposited originally as horizontal layers and was tilted at least 30º down to the SW prior to deposition of paleochannel unit (Ch 3). Subsequent faulting (Rupture Y and/or Z) tilted both the laminated silt (Ls) and paleochannel unit (Ch 3) at least another 15-40º to the SW. Based on the age of the laminated silt unit (Ls) the pre-penultimate earthquake (third oldest) rupture occurred between 690 and 760 AD.

Estimated ages for the three earthquake events observed in this study at Alder Creek overlap estimated earthquake event ages recorded in previous paleoseismic investigations on the North Coast segment of the SAF (Figure 25). The 1906 rupture on the SAF was described in previous trenches on Alder Creek (Baldwin, 1996; and Baldwin et al., 2005), at Scaramella Ranch (Prentice, 1989), and Fort Ross Archae Camp and Orchard sites (Simpson et al., 1996, Kelson et al., 2006).

The penultimate event (rupture Y) in trench T-9 (AD 1440-1640) overlaps well with two interpreted earthquake induced turbidite events, AD 1350-1520 and AD 1510-1670, recorded in cores just offshore to the northwest (Goldfinger et al, 2003). Those particular turbidites are considered to represent the third and fifth oldest earthquakes in a

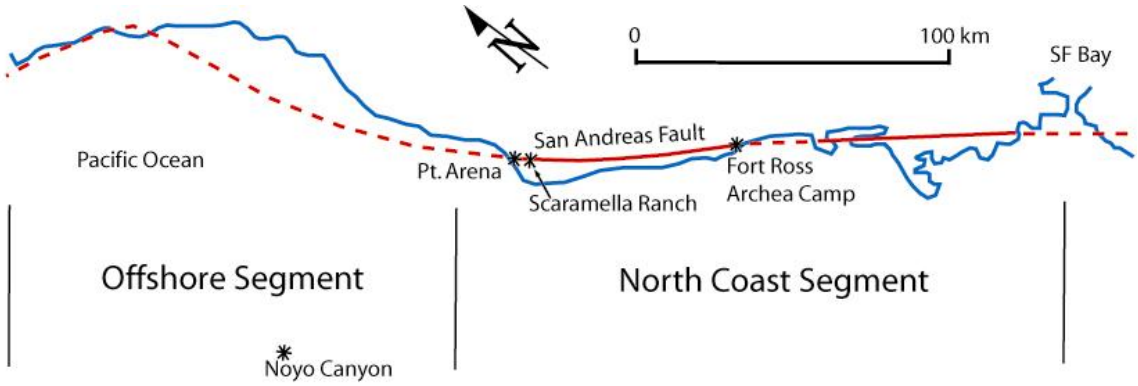

Noyo Canyon (Goldfinger et al., 2007)	Pt. Arena (Baldwin, 1996, Baldwin et al. 2005)	Pt. Arena (This study)	Scaramella Ranch (Prentice, 1989)	Fort Ross, Archea Camp (Simson et al., 1996)
AD 1906	AD 1906	AD 1906	AD 1906	AD 1906
AD 1350-1520 AD 1510-1670	AD 660-1630	AD 1440-1640	AD 1630-1906	AD 1220-1560 AD 1570-1906
AD 700-910 AD 480-700		AD 690-760	AD 400-1300	AD 555-950

Figure 25. Examples of site locations and summary of earthquake events that overlap timing of those found at Alder Creek (Point Arena).

sequence which may include some Cascadia subduction zone events. Similarly, less than 70 km south, at the Fort Ross Archae Camp site, two earthquake events overlap ages associated with rupture Y (AD 1220-1560 and AD 1570-1906) (Simpson et al, 1996, Kelson et al, 2003). Finally, immediately south of this study area, at Scaramella Ranch

(Figure 25), a penultimate event was recorded between AD 1630-1906 (Prentice, 1989) that narrowly overlaps my rupture Y by ten years (Figure 25).

The third oldest event at Alder Creek (rupture Z), AD 690-760, is again within ages that constrain events interpreted at both Noyo Canyon and Fort Ross to the north and south respectively. Two overlapping events, AD 480-700 and AD 700-910, seen in the offshore Noyo Canyon turbidites are in agreement with rupture Z timing (Goldfinger et al., 2003). Goldfinger (2003) interprets those overlapping times to be 7th and 8th oldest events in the SAF record. Rupture Z timing is also in agreement with timing recorded at the Archae Camp, Fort Ross with Simpson's AD 555-950 "event 5".

Microstructure of Alder Creek Samples

Microstructural parameters measured in the Alder Creek paleochannel unit three (Ch 3) sand samples are grain size, grain orientation, and porosity. They record a combination of primary depositional processes and secondary fault-related processes. The objective of part of this research is to identify and describe microstructures that record co-seismic deformation on the SAF.

Grain Size

I have observed that sediment in deformation bands is more fine-grained than sediment away from deformation bands (Figures 17 and 18). I interpret this difference to be grain fracturing and cataclasis processes in deformation bands. SEM images of deformation bands show both cracked and fractured large grains and angular small grains that appear to have formed by fracture and dissaggregation of larger grains (Figure 18).

In contrast, control samples have a more even size distribution and lack fractured or broken grains (Figure 17). I infer that grain-size reduction is compositionally controlled because lithic grains more easily disaggregate with increased strain. In this study, paleochannel unit (Ch 3) sand is composed of approximately 76% lithics. Preferential removal of medium-sized grains is apparent from the cumulative grain size plot (Figure 16). It is also apparent qualitatively, when looking at both control (Figure 17) and deformation band (Figure 18) SEM images.

Porosity

Deformation bands have 9.8-21.6% lower porosity than control samples. This porosity reduction is significant in that it records a combination of both grain rotation and grain breakage within deformation bands. The collapse of pore space records a volume decrease as deformation bands form during coseismic rupture. The accumulation and development of clay within deformation bands also contributes to the lower porosity values.

Grain Orientations

Strong preferred grain orientation in control samples (Figure 17) of paleochannel unit (Ch 3) sand at the Alder Creek site records original signatures of paleoflow direction approximately parallel to the SAF (Figures 4 and 5). Generally, long axes of fluvial clasts, including that of sand grains, dip in the opposite direction of flow (Prothero and Schwab, 1996). The horizontal control sample orientation of N40-70ºW provides the strongest evidence that the creek flowed parallel to sub-parallel to the SAF as it does today at the modern channel location. The 30-50º south-dipping preferred grain

orientation in vertical control sample sand (Figure 17) most likely records both the imbrication (long axes of grains dipping south, transverse to the direction of flow) preserved in Alder Creek's paleochannel unit (Ch 3) and seismic tilting. The east side of the SAF bedding orientation shows that the entire unit has been tilted west side down. Dips of paleochannel unit (Ch 3) sands, measured > 2 m from the SAF in trenches T-10 (Baldwin et al., 2005) and T-10 Peel 1, range from 20-30º SW. This is close to the angle of repose for fluvial sand. Therefore, vertical control samples record up to 30º of tilting, presumably occurring in conjunction with a later slip event (possibly rupture Y).

The stress field across sheared granular layers is heterogeneous; where a network of grain to grain contacts called grain bridges carries the load across the layer. During slip the shear load is accommodated by a networks of grain bridges that hang up on each other, and fail. New bridges then form in their place (Mandl et al, 1977). According to the grain bridge model there are four ways a grain bridge will fail: fracturing of grains, slip between grains, slip between grains and the bounding surface, and through the fracturing of the bounding surface (Sammis and Steacy, 1994).

The grain orientation data from horizontal deformation band sample 4-28 includes two distinct preferred orientations of elongate grains, N10-20ºE and N80ºW (Figure 18). If I assume that grains were originally deposited parallel to sub-parallel to the SAF, as suggested by the control samples, then I interpret the grains oriented N10-20ºE to be a record of approximately 40-50º of clockwise rotation from right lateral shear. The other preferred long axis orientation in horizontal deformation band sample 4-28, N80ºW (Figure 18), probably reflects the point at which grain rotation can no longer be

accommodated. Repeated fracture and crushing results in continued grain bridge failure and tighter packing with smaller grains oriented counter-clockwise at 20-40º. This supports evidence from a previous study that found the long axes of grains within deformation bands in Alder Creek paleochannel unit (Ch 3) sand had a preferred orientation 30º counter-clockwise to the SAF (Cashman et al, 2007).

Vertical sample 4-27, (Figure 18), within the deformation band may reflect a fault parallel alignment of sand grains. The apparent west side up normal motion of the SAF observed in trench T-9, T-10 Peel 1, and T-10 (Baldwin et al., 2005) may be the cause of this vertical grain orientation. The fact that the vertical sample is a two dimensional cross-section (perpendicular to the principle strain direction) of right lateral simple shear obscures any long axis orientations seen in the horizontal sense. If rupture and deformation band propagation starts from below and reaches to the surface during an event, then elongated grains may orient parallel to the rupture.

Summary and Interpretation of Microstructure

The deformation bands in paleochannel unit (Ch 3) sand preserve a coseismic faulting signature. Coseismic deformation realigns grains vertically and horizontally, reduces the grain-size through grain fracturing and disaggregation, and reduces the porosity. It is unclear how much of the primary characteristics of the sand may have affected the fault zone microstructure. The degree to which the original grain orientation affects the post-faulting grain orientation warrants further quantitative investigation.

Microstructures in Experimentally Deformed Sand

This section compares microstructural features observed from shear experiments conducted on Alder Creek sand to those in naturally deformed samples from trench T-9. The experiments were deformed at a confining pressure of 100 KPa, which is roughly equivalent to several meters burial depth at Alder Creek. Features included in this comparison are porosity and grain orientation.

Porosity

Porosity of the samples tested at 100 KPa is approximately 3-12 % higher than porosity within the deformation bands from Alder Creek. This difference is probably due either to the lack of clay accumulation in experimental deformation or to the construction of shearing layers for shear tests. Although shear tests were performed on sand samples from paleochannel unit (Ch 3), most of the original packing and fluvial imbrication in those samples are lost during layer construction. I also carefully enclosed the sand so as not to introduce additional compaction. Therefore, sand in experiments probably had a higher initial porosity than *in situ* sand from paleochannel unit (Ch 3), so the (post-shear test) porosity was higher than that of actual deformation bands.

Grain Orientation

SEM images of samples run at 100 KPa confining pressure indicate pervasive shear extending across the 3 mm width of the sample (Figure 26). Lithic grains show the most significant grain size reduction through fracturing, wear on edges, and disaggregation. This provides evidence that deformation of the sand is compositionally controlled. Quartz and feldspar grains generally only experienced minor fracturing and

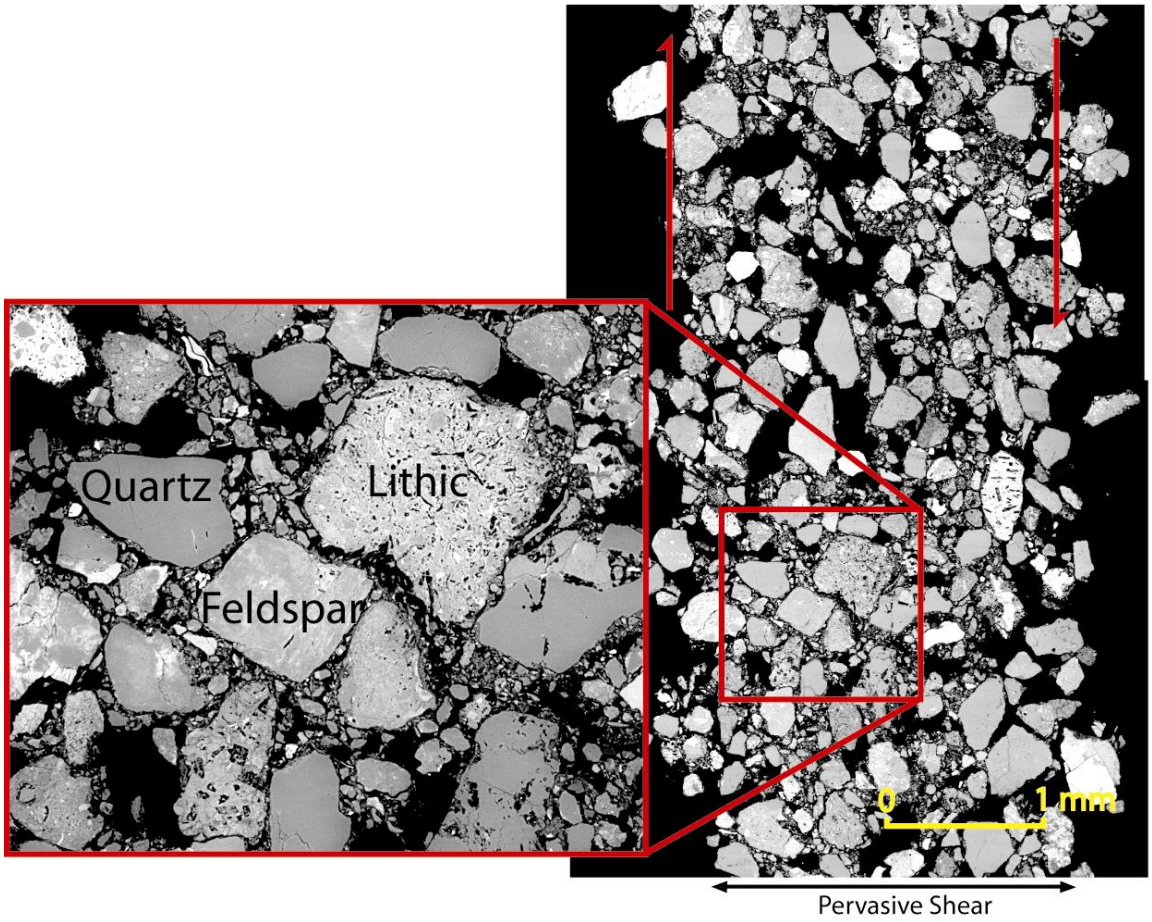

Figure 26. SEM image of sample sheared at 100 KPa. Red arrows indicate the sense of shear and black arrows show the approximate zone of pervasive shear. Representative lithic, quartz, and feldspar grains are identified on the left inset. Shear is relatively pervasive through the width of the sample.

and flaking. Space between grains is partially filled by fine fragments from worn and disaggregated lithic grains.

Rose diagrams and SEM images of the experimental 100 KPa sample resemble those from the horizontal deformation band sample 4-28 (Figures 18 and 23a). Both

exhibit preferred orientations of grains counter-clockwise and parallel to sub-parallel clockwise to the shear sense. This is similar to that observed at the deformation bands. The counter clockwise petals of the 100 KPa rose diagram (Figure 23a) shows grains oriented 30-50º. Sample 4-28 has preferred grain orientation at 50-60º (Figure 18). The lesser population of grains orientated 0-20º clockwise can also be seen in both the 100 KPa rose diagram and that of sample 4-28 (Figures 18 and 23a). Similar to the deformation bands, the mechanism causing two distinct orientations might be repeated grain bridge development and failure.

The 900 KPa samples cannot be directly compared to any field observations or conditions at Alder Creek. However, it is important to note that the SEM image may show the transition of stable to unstable slip behavior as localized shear (Figure 27).

Summary and Interpretation of Microstructure in Experimentally Deformed Sand

Observations of microstructures in experimentally sheared sand samples may help interpret microstructures in natural deformation bands. The porosities are comparable (+3%) to significantly higher (+12%) in experiments to those of deformation bands. Grain orientations of laboratory sheared sand agree with those of naturally-formed deformation bands in the trench (Cashman et al., 2007). Preferred grain orientation occurs from 20º clockwise to 45º counter-clockwise to the sense of shear (right lateral) conducted during the experiment.

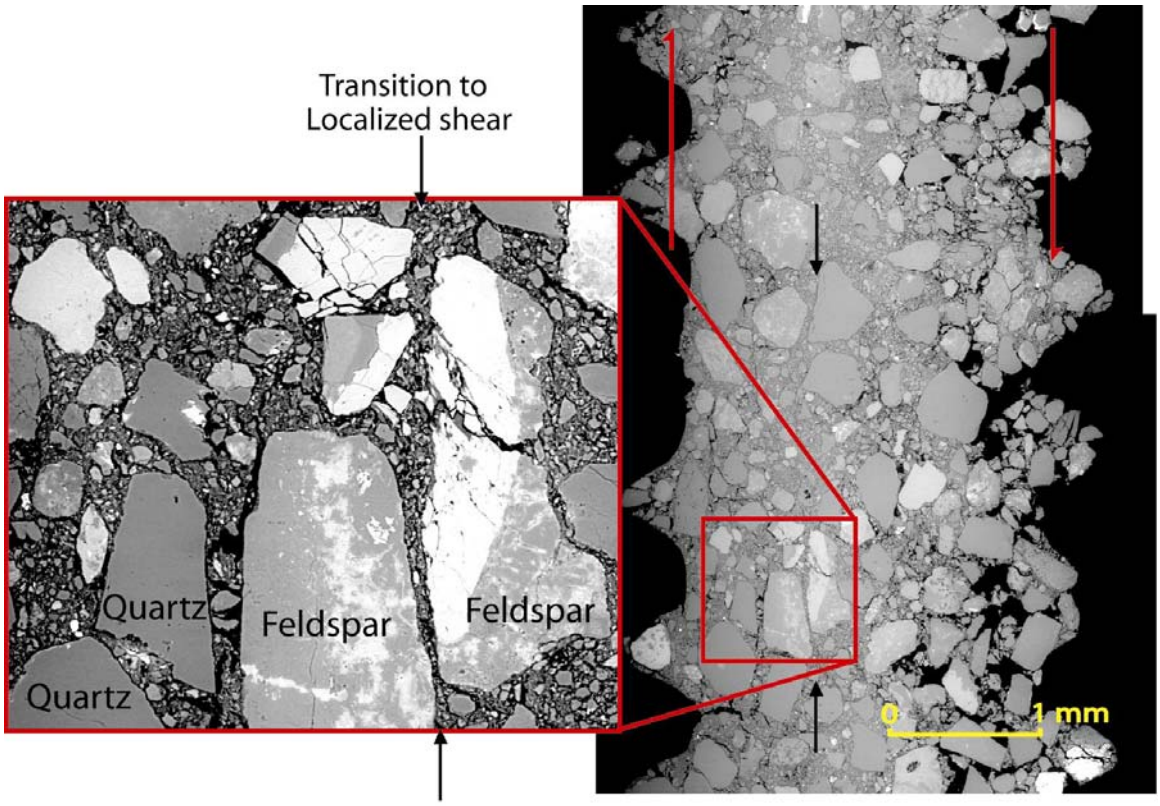

Figure 27. SEM image of sample sheared at 900 KPa. Red arrows indicate the sense of shear and black arrows show approximate zone of localized shearing. Note the remaining larger grains are feldspar and quartz.

Interpretation of Rock Mechanics

The sliding coefficient of friction, μ, is one of the first-order aspects of shallow earthquakes reproducible in laboratory experiments (Marone, 1998). Significantly higher coefficient of friction values (of μ up to 0.57) have been observed in experimentally sheared layers consisting of angular quartz grains and rough boundary conditions

compared to those of smooth grains (0.45) and rough boundary conditions (Anthony and Marone, 2005). Friction increases linearly with an increase in particle angularity and is insensitive to velocity and normal stress variations (Anthony and Marone, 2005). Under similar experimental conditions, μ values for Alder Creek sand are comparable to those observed by Anthony and Marone (2005) in samples with more than 30% angular grains. Both sets of experiments produced stable slip. As the paleochannel unit (Ch 3) sand samples are progressively sheared the reduction in grain-size through fracturing and disaggregation adds a supply of smaller angular grains to the matrix between larger grains. This process increases frictional strength by reducing inter-granular slip.

The increase or decrease in μ, with a sliding velocity increase (velocity jump) is the result of frictional velocity dependence on the a-b parameter (second order). For instance, if a material exhibits a frictional resistance increase (positive values) when sliding velocity increases, this behavior is considered velocity-strengthening (Marone, 1998). Alternatively, a material that shows a reduction (negative values) in frictional resistance with an increase in velocity it is considered velocity-weakening (Marone, 1998). The positive values of a-b in Alder Creek sand at all values of normal stress demonstrate such a velocity-strengthening behavior (Figure 21). This steady decrease in a-b values with increasing normal stress suggests a transition to velocity-weakening behavior might occur at a normal stress around 1000 KPa (Figure 21).

The fact that Alder Creek sand exhibits velocity-strengthening behavior at near-surface conditions has important implications. It agrees with a synoptic model for

earthquake afterslip on mature strike-slip crustal fault zones in that: unconsolidated fault gouge at the surface should have velocity strengthening behavior, and friction rate dependence (a-b) within that fault zone is a function of increased normal stress at depth (Marone, 1998). Fault gouge experiments demonstrate that stable frictional behavior (a-b > 0) is associated with pervasive shearing and velocity strengthening, while unstable velocity weakening frictional behavior (a-b < 0) has been correlated with localized shear (Mair et al., 2002b). The change of the (a-b) value in Alder Creek sand may represent a shift in the micromechanics of strain accommodation from crushing and fracturing to localized slip between individual grains. It has been proposed that the transition from crushing to slip or velocity strengthening to velocity weakening occurs as grain-size distribution becomes wider and more fractal (Sammis and Steacy, 1994).

Distributed shear observed from one rough boundary to the next (initially 5 mm) in the 100 KPa experiment is analogous to shear in deformation bands in the trench. No significant shear occurs outside the deformation band. In the trench, the discrete zone of coseismic rupture represents the width of one or more deformation bands where distributed shear occurs (within the boundaries of 2-10 mm of sand).

The subtle decrease in shear stress during displacement (Figure 22) also indicates that both stable sliding and compaction occurred during the experiments (Anthony and Marone, 2005, Marone, personal comm., 2006). This observed frictional behavior during shear experiments on Alder Creek sand supports the observed porosity reduction in the deformation bands of T-9 and T-10 (Baldwin et al., 2005, Cashman et al., 2007). This

frictional behavior in the Alder Creek sand also supports the conclusion of Anthony and Marone (2005) that both stable sliding and compaction occur when sediment containing greater than 30% angular grains is sheared.

The Mohr law of failure for rocks from shear indicates that the slope of the line relating shear stress as a function of normal stress (Figure 19) is the angle of internal friction (Davis and Reynolods, 1996). The 27.2º angle of internal friction found for experimentally deformed Alder Creek sand is slightly lower than what one would expect to find in loose sand, where loose sand is generally around ~30º and compacted sand ~35º (Davis and Reynolods, 1996). Biegel et al. (1989) report that the angle of internal friction is reduced in simulated fault gouge as it becomes more fractal in grain-size distribution. In other words, fragments that are increasingly surrounded by fragments of various sizes are more likely to fail by slip, thus reducing the angle at which the material will fail. In turn, the friction rate parameter "a" (the increase in μ with increased shear velocity) will slightly decrease as this occurs (Sammis and Steacy, 1994).

CONCLUSIONS

Trenches at Alder Creek expose the active San Andreas fault trace. The presence of upward deformation band shears, subtle shears in soil, and an angular unconformity provide possible evidence for three surface ruptures. Deposits in trenches are correlated based on lithology, stratigraphic relations, and radiometric analysis from this and previous studies conducted at Alder Creek. Based on these relationships and 2-sigma statistical comparisons of radiocarbon dates, the three surface ruptures presented here occur with ranges: AD 1906, AD 1440-1640, and AD 690-760. These three ruptures overlap timing of ruptures observed in previous studies on the North Coast segment of the San Andreas fault, and in the offshore turbidite record.

This study examines outcrop-scale and micro-scale deformational features in sediments deformed at very low confining pressure (near-surface conditions) during coseismic slip along the San Andreas fault. Many of the fault strands in the near surface sediments at Alder Creek are deformation bands. In particular, deformation band sand exhibit preferential grain orientations different than control samples. Sand grain orientations in deformation band and control samples are statistically unique populations. Deformation bands have experienced both porosity reduction and a compositionally controlled fragmentation of grains in comparison to control sands. Qualitatively, grain-size and orientation in a deformation band may reflect a certain process where smaller, angular grains and fragments orient counter-clockwise and larger grains orient parallel to sub-parallel (clockwise) relative to right lateral shear. These observations support the

model of micro-mechanical deformation where continuous grain bridge development and grain bridge failure occurs (Sammis and Steacy, 1994).

Observations of microstructures and frictional behavior of experimentally sheared sand samples taken away from the SAF may help interpret deformation band behavior. When the confining pressure and boundary conditions of laboratory and field samples are comparable, microstructures are similar. Laboratory sheared sand grain orientations match those formed in natural deformation bands (Cashman et al., 2007). The final size and orientation of the experimentally sheared sand are similar to those observed in natural deformation bands. Smaller angular grains and fragments orient counter clockwise and larger grains orient parallel to clockwise sub-parallel relative right lateral shear.

The presence of deformation in near-surface sediments at Alder Creek may be due to composition. Compositional control of deformation band formation in unconsolidated sediment was first recognized by Rawling and Goodwin (2002). This study supports assertions that lithic grains are relatively weak, and that extensive brittle lithic deformation is a mechanism for the abrupt grain-size decrease in Alder Creek deformation bands (Cashman et al., 2007). At Alder Creek, the sand is dominated by lithic grains. SEM images of deformation bands formed in the SAF and in experiments indicate that lithic grains are commonly fractured and disaggregated, while quartz and feldspar grains are less frequently affected.

Experimentally sheared Alder Creek sands exhibit a velocity-strengthening behavior (stable slip) at near surface conditions and velocity-weakening (unstable slip) at

conditions equivalent to burial depths > 45 m. This sand has a relatively high coefficient of sliding friction, yet a slightly lower angle of internal friction. As this material undergoes a change from stasis to slip there is significant grain-to-grain contact and repeated grain bridge formation and failure, grain long axis realignment, and compaction. The velocity strengthening, strain-hardened property of sheared sands makes subsequent faulting likely to occur on new fault strands rather than by additional slip on pre-existing deformation bands. Strain might be accommodated through weaker, more porous sands. This would explain why fault zone deformation bands have a branching and anastomosing nature.

REFERENCES

Anthony, J.L.and C. Marone, 2005. Influence of particle characteristics on granular friction, *Journal of Geophysical Research,* Vol. 110, B08409, p. 1-14.

Antonellini, M., and A. Aydin, 1994. Effect of faulting on fluid flow in porous sandstones: petrophysical properties. *American Association of Petroleum Geologists Bulletin* 78, p. 355-377.

Aydin, A., 1978. Small faults formed as deformation bands in sandstone, *Pageoph*, Birkhauser Verlag, Basel, Vol. 116, p. 913-939.

Baldwin, J.N., 1996. Paleoseismic investigation of the San Andreas fault on the north coast segment, near Manchester, California: M.S. thesis San Jose State University, 127 p. plus plates.

Baldwin, J.N., A.D. Barron, S. Cashman, J.B. Harris, and K.I. Kelson, 2002. Preliminary paleoseismic and geophysical investigation of the North Farrenburg lineament: primary tectonic deformation associated with the New Madrid North fault?, *Seismological Research Letters*, Vol. 73, No. 3.

Baldwin, J.N., S. Cashman, R. Crawford, A. Deis, and K. Cashman, 2005. Deformation band shear zones formed in unconsolidated sediment from repeated Late-Holocene coseismic deformation along the 1906 rupture trace of the San Andreas fault, *American Geophysical Union* 2005 Fall Meeting, abstract #S41B-0996.

Biegel, R.L., C.G. Sammis, and J.H. Dieterich, 1989. The frictional properties of simulated gouge having a fractal particle distribution, *Journal of Structural Geology*, Vol. 11, p. 827-846.

Blake Jr., M.C., and D.L. Jones, 1981. The Franciscan assemblage and related rocks in northern California: a reinterpretation, in Earnst, W.G., ed., *The Geotectonic Development of California*, Rubey Volume I: New Jersey, Prentice-Hall, Inc., p. 307-328.

Blake Jr., M.C., R.W. Graymer, and R.E. Stamski, 2002. Geologic map and map database of western Sonoma, northernmost Marin, and southernmost Mendocino Counties, California, *United States Geological Survey Miscellaneous Field Studies Map* MF-2402.

Brown, R.D., and E.W. Wolfe, 1972. Map showing recently active breaks along the San Andreasfault between Point Delgada and Bolinas Bay, California: Miscellaneous Geologic Investigation Map I-692, *United States Geolological Surv*ey, scale 1:24,000.

Cashman, S., and K. Cashman, 2000. Cataclasis and deformation band formation in unconsolidated marine terrace sand, Humboldt County, Ca., *Geology* 29, p. 111-114.

Cashman, S., J.N. Baldwin, K.V. Cashman, K. Swanson, and R. Crawford, 2007. Microstructures developed by coseismic and aseismic faulting in near-surface sediments, San Andreas Fault, California, Geology, G23545.

Davenport, C.W., 1984. Geology and geomorphic features related to landsliding, Point Arena 7.5' Quadrangle, Mendocino County, Ca. Scale 1:24,000, *United States Geological Survey*, DMG Open-File Report 84-46.

Davis, G. H., and S.J. Reynolds, 1996. Structural Geology, of rocks and regions, John Wiley and sons, Inc., New York, p. 317, 308-309, and 546-549.

DeMets, Charles, R.G. Gordon, Stein, Seth, and D.F. Argus, 1987. A revised estimate of Pacific- North America motion and implications for western North America plate boundary zone tectonics: Geophysical Research Letters, Vol. 14, no. 9, p. 911-914.

Galehouse, J.S., 2002. Data from theodolite measurements of creep rates on San Francisco Bay region faults, California: 1979–2001, *United States Geological Survey*, Open-File Report 02–225.

Goldfinger, C., C. H. Nelson, J.E. Johnson and Shipboard Scientific Party, 2003: Holocene earthquake records from the Cascadia subduction zone and northern San Andreas Fault based on precise dating of offshore turbidites. *Annual Review of Earth and Planetary Science* 31, p. 555-577.

Hirauchi, K., and K. Hisada, 2004. Structural Analysis of Serpentinite in the Jikkoku Pass Area, Northwestern Kanto Mountains, Central Japan, *American Geophysical Union*, Fall Meeting 2004, abstract #T51A-0443.

Johansen, I.A., and R. Bürgmann, 2005. Creep and quakes on the northern transition zone of the San Andreas fault from GPS and InSAR data, *Geophysical Research Letters*, 32.

Kelson, K.I., A.R. Streig, R.D. Koehler, and K. Kang, 2006. Timing of Late Holocene Paleoearthquakes on the Northern San Andreas Fault at the Fort Ross Orchard Site, Sonoma County, California, *Bulletin of the Seismological Society of America*; June 2006; Vol. 96; No. 3; p. 1012-1028.

Kirkman, T.W., 1996. Statistics to Use. http://www.physics.csbsju.edu/stats/ (November 15, 2006)

Lawson, A.C., 1908. The California earthquake of April 18, 1906, Report of the state earthquake investigation, Carnegie Institute Washington Pub. 87. p. 451.

Mair, K., S. Elphic, and I. Main, 2002a. Influence of confining pressure on the mechanical and structural evolution of laboratory deformation bands, *Geophysical Research Letters*, Vol. 29, No. 10.

Mair, K., K. Frey, and C. Marone, 2002b. Influence of grain characteristics on the friction of granular shear zones, *Journal of Geophysical Research*, Vol. 107, No. B10, 2219.

Mandl, G, L.N.J. Dejong, and A. Maltha, 1977. Shear zones in granular material: An experimental study of their structural and mechanical genisis, *Rock Mechanics*, Vol. 9, p. 95-144.

Marone, C., 1998. Laboratory-derived friction laws and their application to seismic faulting, *Annual Review of Earth Planet Science*, 26, 643-696.

Marone, C, 2006. Personal communication at the Penn State Rock Mechanics laboratory, e-mail and by telephone.

Prentice, C.S., 1989. earthquake geology of the northern San Andreas fault near Point Arena, California: Pasadena, California, California Institute of Technology, PhD Dissertation.

Prothero, D.R., and F. Schwab, 1996. Sedimentary Geology, An introduction to sedimentary rocks and stratigraphy, W. H. Freeman and Company, New York, p. 92.

Rawling, C.G., and L.B. Goodwin, 2002. Cataclasis and particulate flow in faulted, poorly lithified sediments, *Journal of Structural Geology*, 25, p. 317-331.

Sammis, C.G., and S.J. Steacy, 1994. The micromechanics of friction in a granular layer, *Pageoph.* Vol. 142, No. ¾, 777-794.

Simpson, G.D., J.S. Noller, K.I. Kelson, and W.R. Lettis, 1996. Logs of trenches across the San Andreas fault, Archae camp, Fort Ross State Historic Park, Northern California: *United States Geological Survey* NEHRP Final Technical Report.

Stuiver, M., and P.J. Reimer, 1998. Radiocarbon calibration program, CALIB rev. 5.0.1, *Radiocarbon* 35, 285-295.

Thatcher, W., G. Marshall, and M. Lisowsk, 1997. Resolution of fault slip along the 470-km-long rupture of the great 1906 San Francisco earthquake and its implications. *Journal of Geophysical Research*, Vol. 102, No. B3, p. 5353–5368.

Thatcher, W., 2006. Present-day crustal movements and the mechanics of cyclical deformation, The San Andreas Fault system, California. *United States Geological Surv*ey Professional Paper 1515.

Wallace, R.E., 1990. The San Andreas fault system, California: U.S. Geological Survey Professional Paper 1515, 283pp.

Working-Groups on California Earthquake Probabilities (WGCEP), (2003). Earthquake probabilities in the San Francisco Bay region: 2002-2031-a summary of findings, *United States Geological Survey* Open-File Report *03-214.*

Yagi, Yuji, Kikuchi, and Masayuki, 2000. Source rupture process of the Kocaeli, Turkey, earthquake of August 17, 1999, obtained by joint inversion of near-field data and teleseismic data, *Geophysical Research Letters*, Volume 27, Issue 13, p. 1969-1972.